SMA Newsletter

Submillimeter Array Newsletter | Number 19 | January 2015

CONTENTS

FROM THE DIRECTOR

Dear SMA Newsletter readers,

Last year we introduced a new class of large-scale observational projects, those that require many nights observing over multiple semesters. Last semester we started the first such project: *The SMA Legacy Survey of the Central Molecular Zone*, (PI Eric Keto) and this semester we began a second: *Mass Assembly of Stellar Systems and their Evolution with the SMA* (PI Michael Dunham). Subsets of the data from these large scale projects will be made available through the SMA data archive before all observations are complete, and we expect to release the entire body of data at the end of the semester that follows project completion – in contrast to the usual 15-month proprietary data period. We also expect that fully-reduced data sets from these two projects will be made publicly available within one year of project completion. Each of these projects will span three observing semesters, and will require 50 – 60 nights of telescope time. Consequently, time available for other projects will be reduced near the hour angles centered at 17 and 04 hours associated with these projects. For the next two semesters proposals that avoid these hour angles will have the best chance of receiving time.

For the past few months we have often been observing an additional 1 GHz (per sideband) as we commission the SWARM correlator, and a number of observing proposals have been completed using this additional bandwidth. Many projects will benefit from the increase in sensitivity and spectral coverage gained by the addition of SWARM to the legacy ASIC correlator. Unfortunately, there will be no impact on the time required to complete the two legacy projects mentioned above. As SWARM is fully commissioned and subsequently expanded, we look forward to the increase in the SMA's scientific productivity.

Ray Blundell

MAGNETIC FIELDS IN THE FORMATION OF MASSIVE PROTO-CLUSTERS

K. Qiu[1], Q. Zhang[2], K. M. Menten[3], H. B. Liu[4], Y.-W. Tang[4] & J. M. Girart[5]

Massive Stars (stellar mass > $8M_{\odot}$) tend to form in clusters, which arise from the gravitational collapse and fragmentation of molecular clouds. In this process, the key question under debate is that which mechanism, turbulence or magnetic fields, plays a central role in counteracting with gravity. In the scenario of gravo-turbulent fragmentation, supersonic turbulence produces a hierarchy of density structures; as turbulence decays locally, gravitational collapse sets in to give birth to a proto-cluster. Stars near the cloud center could accrete gas at a higher rate, thus they end up being more massive. Magnetic fields are implicitly weak in this scenario, and are predicted to exhibit a chaotic morphology due to turbulent and dynamical twisting (Padoan et al. 2001). In contrast, magnetic fields are crucial in the classic theory of isolated low-mass star formation. The theory assumes that molecular clouds are magnetically supported; in collapsing cores where star formation takes place, magnetic fields are pulled by gravity into an hourglass shape (Crutcher 2006). Cores contract more along magnetic fields, resulting in a flattened morphology perpendicular to the field axis, and a bipolar outflow is magnetically driven along the field axis from an accretion disk embedded within the core.

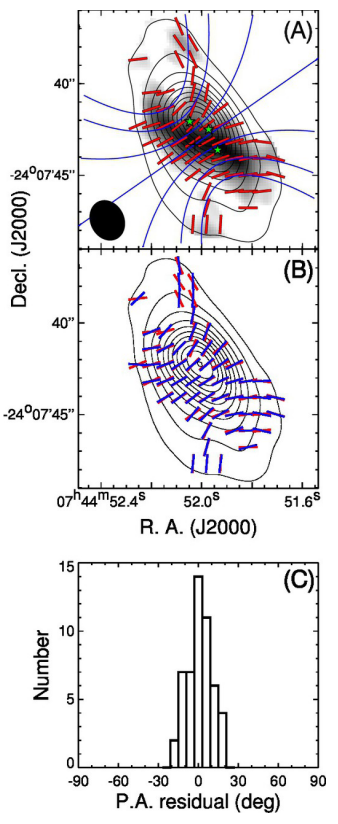

Figure 1: (A) Contour map of the 880 μm dust emission superposed on the gray scale image of the polarized intensity stretching from 2.2 to 7.1 mJy/beam. Contour levels are $15\times(1,2,3...11)^{1.5}$ mJy/beam. Red bars indicate the orientation of the magnetic field. Blue lines show the parabolic shape of the best-fit model. Three star symbols mark protostellar condensations seen in previous observations (Qiu et al. 2009). The synthesized beam is shown in the lower left. (B) Contours and red bars are the same as in (A). Blue bars correspond to the best-fit model. (C) Histogram of the polarization angle residuals for the best-fit model.

As part of the SMA Legacy Project dedicated to probing the role of magnetic fields in massive star formation (Zhang et al. 2014), we carried out polarization observations in dust continuum and molecular lines toward G240.31+0.07 (G240) in sub-compact, compact, and extended configurations (Qiu et al. 2014). G240 is a massive star-forming region best known for a well-shaped bipolar outflow originating from a massive and flattened core which is fragmenting to form a high-mass proto-cluster (Qiu et al. 2009). In **Fig. 1A**, the magnetic field threading the core is inferred from the linearly polarized dust emission. The field morphology exhibits a clear hourglass shape with its axis perpendicular to the flattened core. We fit the magnetic field with an analytical model of a series of parabolic functions. The best-fit model agrees well with the measured magnetic field, with the residuals showing a nearly Gaussian distribution **(Figs. 1B and 1C)**.

The magnetic field axis is aligned within 20° of the axis of the bipolar outflow **(Fig. 2)**. We examine the simultaneously observed spectral lines to investigate the kinematics of the dense core. In Fig. 2, the $H^{13}CO^+$ (4-3) emission reveals a velocity gradient along the major axis of the core. The velocity gradient is also seen in other high-density tracing spectral lines, and provides strong evidence for a rotating motion. We perform a linear fit to the peak positions of the $H^{13}CO^+$ emission in each velocity channel to

[1]School of Astronomy and Space Science, Nanjing University, 163 Xianlin Avenue, Nanjing 210023, China. [2]Harvard-Smithsonian Center for Astrophysics, 60 Garden Street, Cambridge, MA 02138, USA. [3]Max-Planck-Institut für Radioastronomie, Auf dem Hügel 69, 53121 Bonn, Germany. [4]Academia Sinica Institute of Astronomy and Astrophysics, P.O. Box 23-141, Taipei 10617, Taiwan. [5]Institut de Ciències de l'Espai (CSIC-IEEC), Campus UAB, Facultat de Ciències, C5p 2, E-08193, Bellaterra, Catalonia, Spain.

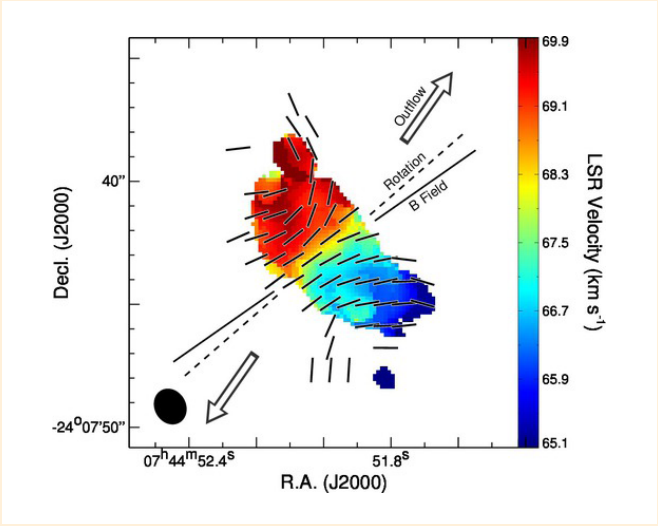

Figure 2: Color image shows the flux weighted velocity map in $H^{13}CO^+$ (4-3). Black bars indicate the orientation of the magnetic field. Two thick arrows show the direction of the bipolar outflow (Qiu et al. 2009); dashed lines show the rotation axis; and solid lines show the axis of the magnetic field.

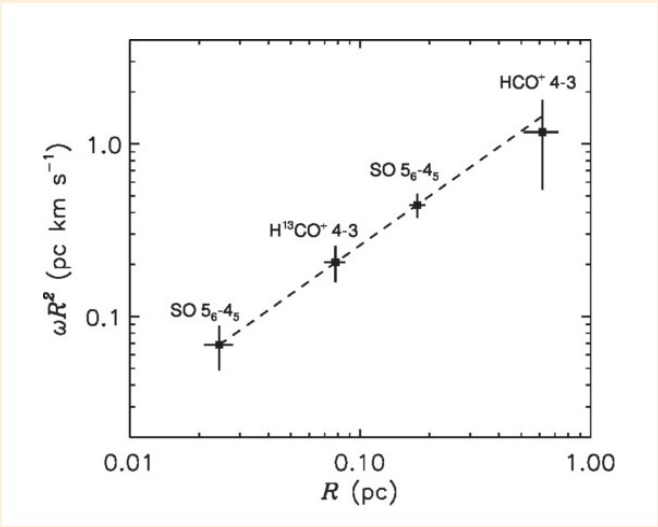

Figure 3: The distribution of the specific angular momentum as a function of the radius. Dashed line shows the power-law fit: $\omega R^2 = 10^{0.35\pm0.10} R^{0.95\pm0.07}$.

gauge the orientation of the rotation axis, and find it to be only 6° offset from the magnetic field axis.

We estimate the strength of the magnetic field with the Chandrasekhar-Fermi method (Ostriker et al. 2001). Alternatively, since the magnetic field is being pulled by gravity, we can calculate the magnetic field strength from the observed curvature of the field lines (Schleuning 1998). For G240, the two estimates are consistent with each other, and yield a field strength of about 1 mG. We then assess the significance of the magnetic field with respect to the gravity, turbulence, and centrifugal force. The mass-to-magnetic flux ratio determines whether a magnetically supported cloud would collapse under its self-gravity. In G240, the ratio is about 1.4 times the critical value, thus the core is slightly supercritical, implying that the gravity has started to overcome the magnetic force. Assuming that turbulence is the only source of the intrinsic dispersion in the polarization angle, the turbulent to magnetic energy ratio is estimated to be 0.4. So the ordered magnetic energy dominates over the turbulent energy.

We further investigate the property of the rotating motion with new observations of SO (5_6-4_5) made with the SMA and HCO^+ (4-3) made with the Atacama Pathfinder EXperiment. A velocity gradient consistent with what is shown in Fig. 2 is found on all the scales explored. In **Fig. 3**, the specific angular momentum, ωR^2, decreases toward the center, and a power-law fit to the data yields a $R^{0.95\pm0.07}$ dependence. We speculate that the decrease in ωR^2 is mostly attributed to magnetic braking. Numerical studies show that magnetic braking acts to align the rotation axis to the magnetic field, while the centrifugal force causes the magnetic field to incline: if the ratio of the angular velocity to the magnetic field strength, ω/B, is smaller than a critical value, $0.39G^{1/2}/c_s$, where c_s is the sound speed, magnetic braking is overwhelming, otherwise, the centrifugal force wins (Machida et al. 2006). In

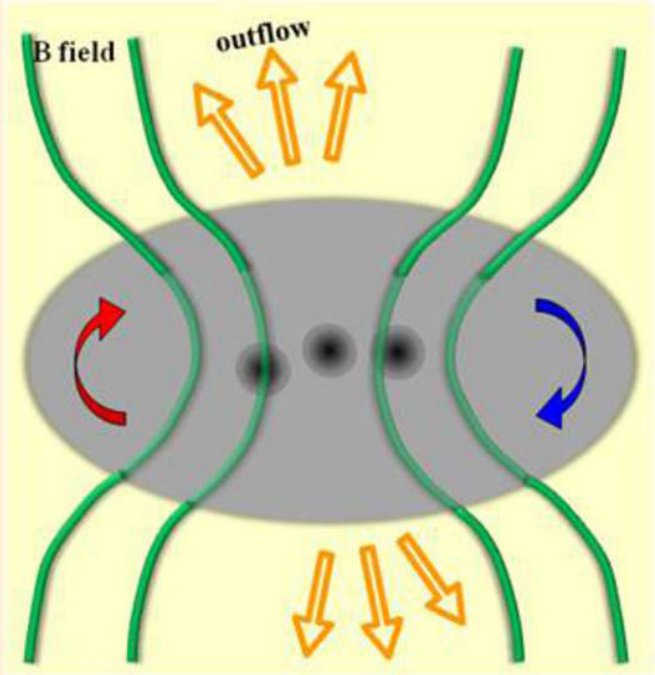

Figure 4: Schematic view of the magnetic field and kinematics observed in G240. The core (gray-filled ellipse), which is flattened and rotating (blue and red arrows indicate the sense of the rotation), is threaded by an hourglass magnetic field. The field is largely aligned with a bipolar outflow, which is likely driven from the central of three protostellar condensations (dark gray dots).

G240, the rotation axis of the core (and even that of an embedded disk from which the outflow originates) is aligned with the magnetic field, suggesting that magnetic braking is more important. Indeed, ω/B is found to be 2.4×10^{-8} year^{-1} μG^{-1}, clearly smaller than the critical value of 9.7×10^{-8} year^{-1} μG.

We summarize the observed magnetic field and kinematic properties in G240 in **Fig. 4**. This picture is surprisingly consistent with the theoretical predictions of the classic paradigm of isolated low-mass star formation, except that G240 is a massive core and shows a higher degree of fragmentation. It is the first time that a clear hourglass magnetic field aligned with a well-defined outflow is detected in the high-mass regime. The observations provide strong evidence that massive star and cluster formation in G240 is proceeding in a way similar to the formation of Sun-like stars. We also find that the magnetic field energetically dominates over turbulence in shaping the dynamics. The nearly linear decrease in the specific angular momentum suggests that magnetic braking is at work and overcomes the centrifugal force.

REFERENCE

- Crutcher, R. M. 2006, Science, 313, 771
- Padoan, P. et al. 2001, ApJ, 559, 1005
- Zhang, Q. et al. 2014, ApJ, 792, 116
- Qiu, K. et al. 2014, ApJ, 794, L18
- Qiu, K. et al. 2009, ApJ, 696, 66
- Ostriker, E. C. et al. 2001, ApJ, 546, 980
- Schleuning, F. A. 1998, ApJ, 493, 811
- Machida, M. N. et al., 2006, ApJ, 645, 1227

THE DYNAMICS AND STAR-FORMING POTENTIAL OF THE MASSIVE GALACTIC CENTER CLOUD G0.253+0.016

Katharine Johnston (University of Leeds, UK) and Henrik Beuther (MPIA, Germany)

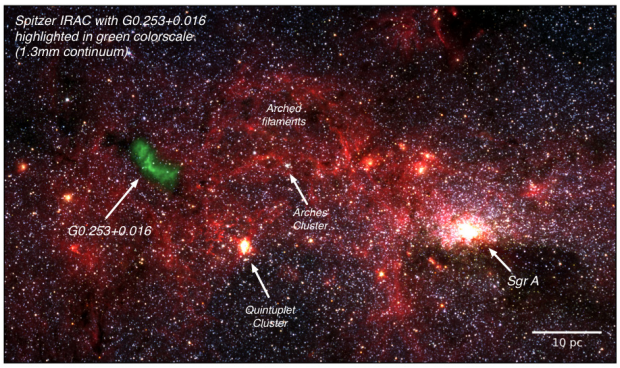

Figure 1: A three-color (red/green/blue = 8/4.5/3.6 micron) *Spitzer* IRAC composite view of the inner Central Molecular Zone (CMZ) with 1.3mm continuum emission from G0.253+0.016, derived from our SMA observations, highlighted in light green. Several other well-known features of the CMZ are labeled. *Spitzer*/IRAC credit: NASA/JPL-Caltech/S. Stolovy (Spitzer Science Center/Caltech).

At the turn of the millennium, the Midcourse Space Experiment (MSX; Price et al. 2001) unveiled a population of thousands of infrared dark clouds (IRDCs) across the Milky Way (Egan et al. 1998). Further investigation, in which the SMA played a crucial role, determined that these dense ($> 10^5$ cm^{-3}) and cold (< 20 K) clouds were the sites of the earliest stages of massive star and cluster formation. In particular, SMA observations were able to uncover detailed properties of IRDCs, such as their level of fragmentation, turbulence, star-forming content, and chemistry (e.g. Rathborne et al. 2008, Zhang et al. 2009, Wang et al. 2011, 2014).

In our recent study (Johnston et al. 2014), we pointed the SMA toward the exceptional IRDC G0.253+0.016, also known as 'the Brick'. Situated within the Central Molecular Zone (CMZ) – the inner several 100 pc – of the Milky Way, this compact (r < 5 pc) cloud has a mass of ~10^5 $M_\odot$, yet contains few signposts of ongoing star formation associated with the dense gas. **Fig. 1** shows an IRAC three-color composite image of the inner CMZ with the millimeter continuum emission from G0.253+0.016 highlighted. Using 230 GHz SMA observations, we set out to investigate the physical properties, dynamics and structure of this cloud to understand what has inhibited star formation within it. Studying this unusual cloud also allowed us to test further the applicability of predictive "star-formation laws" in the form of critical density thresholds for star formation to clouds in extreme environments such as the Galactic center.

Our observations consisted of the standard SMA 230 GHz setup **(Fig. 2)**, allowing us to observe a range of lines as well as the dust continuum over a bandwidth of 2 GHz. Many of the lines that were detected, such as SiO, SO, methanol and HNCO, are shock-tracing species, whereas – although covered by our observations – the hot core tracer CH_3CN was

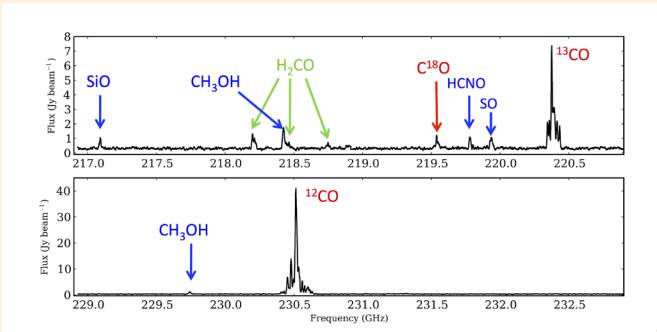

Figure 2: Observed SMA spectrum of G0.253+0.016 in both sidebands, on a short baseline (antennas 1 and 7), and averaged over the six observed fields of the mosaic. Lines labeled in blue are shock-tracing lines, those in red are CO isotopologues and thus trace the diffuse gas, and those in green are formaldehyde lines, which can be used as a temperature probe. (from Fig. 7 of Johnston et al., 2014)

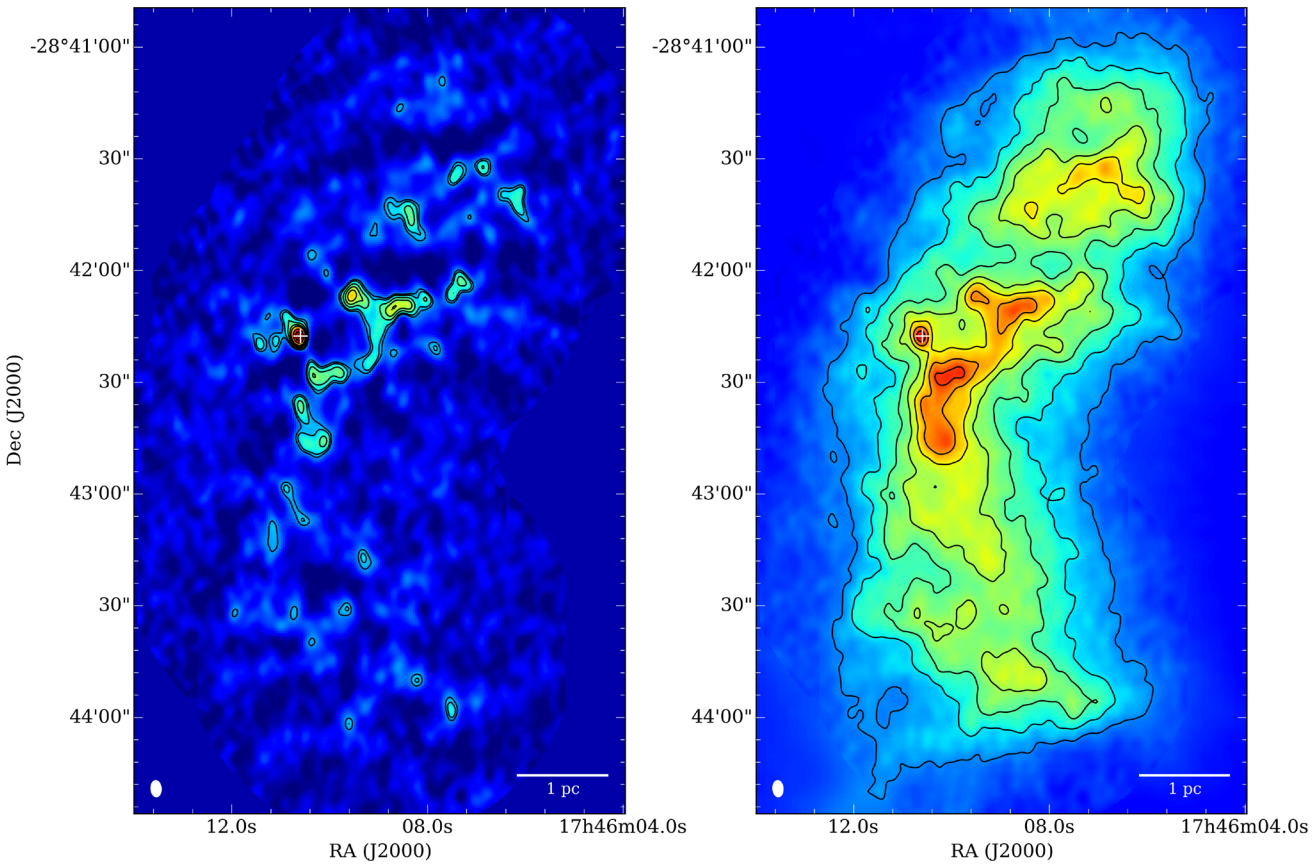

Figure 3 Left: In both colorscale and contours, the 1.3 mm continuum emission from G0.253+0.016 observed with the SMA. **Right:** The SMA 1.3mm emission combined with SCUBA single-dish data, providing an excellent view of both the large and small-scale structure within the cloud. The plus sign in both panels marks the water maser reported by Lis et al. (1994). (adapted from Figs. 2 and 4 of Johnston et al., 2014)

not detected, indicating that massive star formation is not widespread or particularly evolved throughout the cloud.

Our SMA continuum observations at 1.3 mm and 1.37 mm detected 36 dust cores within G0.253+0.016 with masses between 25 and 252 $M_\odot$ and column densities ranging from 0.4 x 10^{23} cm^{-2} to 2 x 10^{23} cm^{-2}. To recover both the large-scale emission from the cloud as well as the structure traced by the SMA, we combined our SMA image **(Fig. 3, left)** with a single-dish image of the 1.3mm emission derived using SCUBA and *Herschel* continuum data. The resulting map is shown in **Fig. 3 (right)**.

Using this combined map, we derived column densities across the cloud and determined that the probability distribution function of the column density (N-PDF) within G0.253+0.016 is log-normal with no obvious power-law tail at higher densities. When accounting for increased turbulence and magnetic field strengths observed in the CMZ, this shape as well as the width of the N-PDF is in good agreement with current theory predicting the density structure of molecular clouds shaped by supersonic magnetized turbulence (e.g. Molina et al. 2012). In addition, the missing power-law tail confirms the assessment of barely any ongoing star formation.

As well as investigating the N-PDF of G0.253+0.016, we derived the Δ-variance spectrum of the cloud, which can be directly related to its density power spectrum. Again we found that most of the structure in the cloud is on large scales, in accord with theoretical predictions of the Δ-variance spectrum for quiescent clouds with a low instantaneous star-formation efficiency (Federrath et al. 2013).

The set of lines that we observed also allowed us to determine the kinematics and kinetic temperatures within the cloud. We observed broad linewidths and the brightest shock tracer emission in the south of the cloud. Furthermore, a position-velocity diagram of the cloud shows the brightest shock tracing emission exists at the boundary in velocity between G0.253+0.016 and another cloud at v_{LSR} ~ 70 kms^{-1}. In addition, the kinetic temperature of the gas that we derived from H_2CO line ratios is > 320 K on size-scales of the SMA beam (~0.15 pc), consistent with the cloud being heated on small scales by shocks.

Recently, Kauffmann et al. (2013) determined that column density thresholds for star formation derived from nearby clouds (Lada et al. 2010, Heiderman et al. 2010) are inconsistent with the lack of star formation in G0.253+0.016. In addition to this, we found that even after

scaling the column density threshold for star formation to account for the high level of turbulence in CMZ clouds, ten forming stars with masses > 15 $M_\odot$ should still be detectable within the cloud, but these are not observed.

A number of physical aspects may go toward explaining this discrepancy. For instance, the cloud may exist on top of a constant but non-negligible background density which does not contribute to its gravitational binding. In this case, a critical overdensity threshold may be a more appropriate measure of star-forming potential than an absolute density threshold (e.g. Krumholz et al. 2005, Kruijssen et al. 2014, Rathborne et al. 2014b). We also cannot rule out the possibility that we are only observing this cloud in the first throes of star formation, and that later it will fulfill its star-forming potential. However, considering it is probably globally unbound (Kauffmann et al. 2013), and that only a small number of the cores we observed have linewidths that indicate they are bound, G0.253+0.016 may never go on to form a cluster.

REFERENCES

- Egan et al., 1998, ApJ, 494, L199
- Federrath et al. 2013, A&A, 512, A81
- Heiderman et al., 2010, 723, 1019
- Johnston et al., 2014, A&A, 568, A56
- Kauffmann et al. 2013, ApJ, 765, L35
- Kruijssen et al., 2014, MNRAS, 440, 3370
- Krumholz et al., 2005, ApJ, 618, L33
- Lada et al., 2010, ApJ, 724, 687
- Lis et al., 1994, ApJ, 423, L39
- Molina et al., 2012, MNRAS, 423, 2680
- Price et al., 2001, AJ, 121, 2819
- Rathborne et al., 2008, ApJ, 689, 1141
- Rathborne et al. 2014b, ApJ, 795, L25
- Wang et al., 2011, ApJ, 735, 64
- Wang et al., 2014, MNRAS, 439, 3275
- Zhang et al., 2009, ApJ, 696, 268

THE MAXIMUM STAR FORMATION RATE IN HIGH-REDSHIFT GALAXIES

Amy Barger

We now know from far-infrared/submillimeter galaxy studies that there is a large fraction of cosmic star formation hidden by dust, much of which is occurring in the most massively star-forming galaxies in the universe. At high redshifts, these high star formation rate galaxies are almost impossible to pick out in rest-frame UV or optical samples due to their very large and highly variable extinctions (Bouwens et al. 2009; Reddy et al. 2012). Thus, if we are to construct a complete picture of galaxy evolution, we need a full understanding of galaxies at both optical and far-infrared/submillimeter wavelengths.

The primary obstacle in determining the properties of the far-infrared/submillimeter galaxy population is the poor resolution of long-wavelength, single-dish telescopes. Thus, it is critical to follow up sources detected by single-dish telescopes with observations from submillimeter interferometers, such as the SMA. The finer spatial resolution interferometers provide allows identification of counterparts at other wavelengths and can be used to determine whether the detections are blends of fainter sources with lower star formation rates.

We have been carrying out a survey of blank fields with the SCUBA-2 camera (Holland et al. 2013) on the 15 m James Clerk Maxwell Telescope to construct a large sample of high-redshift submillimeter galaxies. SCUBA-2 provides a more efficient way to find distant submillimeter galaxies than the first-generation SCUBA camera. SCUBA-2 covers 50 square arcmin, which is 16 times the area of SCUBA, and it has a mapping speed that is considerably faster due to its filled array. The goals of our SCUBA-2 survey are to determine (1) the highest star formation rates in galaxies, (2) the distribution of star formation rates, and (3) the contribution of submillimeter galaxies to the universal star formation history, as well as how that contribution compares to the contribution from extinction-corrected rest-frame UV selected samples.

In Barger et al. (2014), we presented a uniformly selected sample of 850 micron galaxies in the Chandra Deep Field-North (CDF-N). We found counterparts to many of the submillimeter galaxies in an ultradeep 1.4 GHz image from the upgraded Very Large Array (F. Owen, in preparation). We observed many of our SCUBA-2 sources with the SMA in order to resolve ambiguous cases (i.e., multiple radio sources in the SCUBA-2 beam), to look for blending of fainter submillimeter sources into a single SCUBA-2 source, and to confirm SCUBA-2 sources that had no radio counterparts at all, perhaps due to their extreme redshifts. In **Figure 1**, we show an SMA image of one of the SCUBA-2 sources. There are four radio sources (small circles) in the SMA field, but only one is

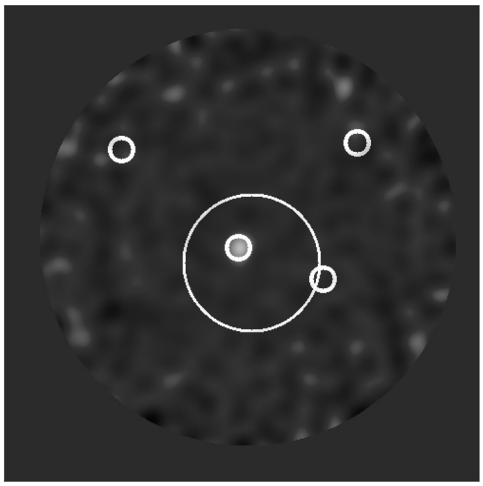

Figure 1: SMA image of CDFN8 with a measured 860 micron flux of 11.5+/-0.7 mJy from the SMA and an 850 micron flux of 9.5+/-2.3 mJy from SCUBA-2. The large circle shows the SCUBA-2 beam centered at the SCUBA-2 position. The small circles show the positions of 1.4 GHz sources in the field. The submillimeter source is a single unresolved source at the position of a 1.4 GHz source with a flux of 34.2+/-2.9 microJy. None of the other three radio sources in the field have a significant submillimeter flux.

the clear counterpart to the SMA source. The other three have no significant submillimeter flux.

Our final sample contained 49 SCUBA-2 sources, 24 of which have SMA identifications (of these, 3 have multiple SMA counterparts, giving a total of 27 SMA detected sources). A further 18 have a single radio source within the SCUBA-2 beam. We calculated star formation rates from both the radio power and the submillimeter flux and found that they approximately agreed (the submillimeter derived star formation rates are about 5% higher, on average). We found that the star formation rates of the submillimeter galaxies ranged from 400 to 6000 solar masses per year. However, we found evidence for a highly statistically significant turn-down in the star formation rate distribution function, indicating a characteristic maximum star formation rate in galaxies of about 2000 solar masses per year.

We compared the star formation rate contributions of the massively star-forming galaxies in our SCUBA-2 sample to those of the Lyman break galaxies or LBGs in the extinction-corrected rest-frame UV selected samples from z~2 to z~5 **(Figure 2)**. While the distribution function appears to extend smoothly from the submillimeter galaxies to the LBGs, the star formation rates of the LBGs are not as high as those of the submillimeter galaxies, but rather cut off at about 300 solar masses per year. This

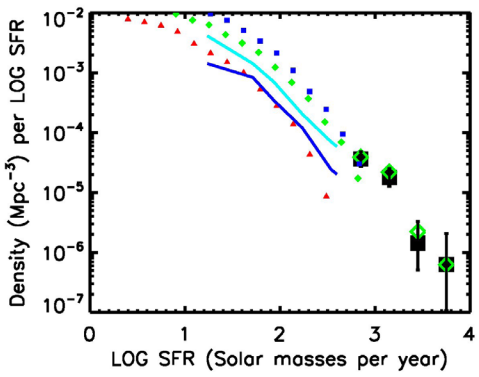

Figure 2: Number density per unit comoving volume per unit log star formation rate vs. log star formation rate for the >4-sigma SCUBA-2 sources at z=1.5-6 with star formation rates >500 solar masses per year. Black squares show the sources with SMA detections or single radio counterparts. The error bars are 68% confidence ranges based on the number of sources in each bin. The green diamonds show the results if the five submillimeter galaxies without radio counterparts are also assumed to lie in this redshift interval. For comparison, the small symbols and curves show extinction-corrected rest-frame UV results from van der Burg et al. (2010) (red triangles - z=4.8; green diamonds - z=3.8; blue squares - z=3.1) and Reddy & Steidel (2009) (blue curve – z~3; cyan curve – z~2), assuming the Kennicutt (1998) conversion of UV luminosity to star formation rate for a Salpeter initial mass function.

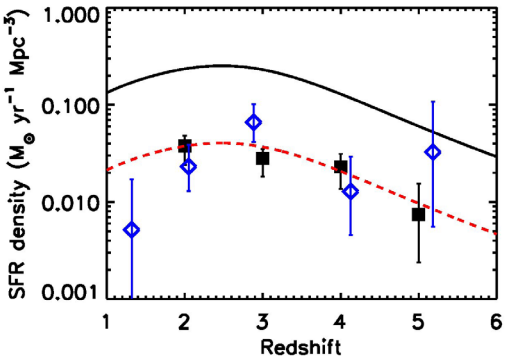

Figure 3: Star formation rate density per unit comoving volume vs. redshift for the SCUBA-2 sample with star formation rates >500 solar masses per year. The black squares show the computations at z=1.5-2.5, 2.5-3.5, 3.5-4.5, and 4.5-5.5 and are plotted at the mean redshift of each bin. Sources without radio counterparts are placed at their minimum millimetric redshifts, and we have renormalized the points by a multiplicative factor of 1.1 to allow for the sources with multiple radio counterparts. The error bars are 68% confidence ranges based on the number of sources in the bin. The black solid curve shows the star formation rate density history computed by Hopkins & Beacom (2006) based on extinction-corrected rest-frame UV selected samples, and the red dashed curve shows this multiplied by 0.16 to match roughly the star formation rate density history of the current sample. The blue open diamonds show the star formation rate density history computed by Barger et al. (2012) based on the smaller SCUBA sample in the GOODS-N field. We have reduced these points by a factor of 1.4 to correspond to the present star formation rate calibration.

means that the two samples are essentially disjoint. This has the important consequence that the star formation rate density history determined for the submillimeter galaxies needs to be added to the star formation rate density history determined for the LBGs for a more complete accounting. Indeed, the star formation contribution determined from the bright submillimeter galaxies in our sample corresponds to about 16% of that determined from the extinction-corrected rest-frame UV (compilation of Hopkins & Beacom 2006), making bright submillimeter galaxies a significant contributor to the overall star formation history, as can be seen from **Figure 3**.

Stacking analyses of SCUBA data found that the brightest submillimeter fluxes of LBGs are only ~0.2-0.3~mJy (Peacock et al. 2000; Chapman et al. 2000; Webb et al. 2003). Meanwhile, the submillimeter sensitivities of our SCUBA-2 survey are set by the blank field confusion limit of 2 mJy, leaving a gap between the LBG and bright submillimeter galaxy populations where the star formation rate distribution function is poorly determined. This regime corresponds to luminous infrared galaxies or LIRGs (L_IR>10^11 L_Sun).

To explore this regime, we have also been observing with SCUBA-2 massive lensing cluster fields, which have the advantage of probing the intrinsically faint fluxes of background sources, since those sources get gravitationally magnified to a detectable level by the presence of the intervening cluster mass, and the source plane gets expanded, which reduces the confusion limit. In Chen et al. (2013), we obtained extremely deep galaxy number counts at 450 micron and 850 micron. We combined data on two cluster lensing fields and three blank fields to measure the number counts over a wide flux range at each wavelength. Based on these number counts, faint submillimeter galaxies contribute about 70% of the 850 micron extragalactic background light, indicating that they are the dominant star-forming galaxy population in the dusty universe. Thus, a full accounting of the star formation history also requires a thorough understanding of the faint submillimeter galaxy population.

In particular, we need to determine whether the contributions from faint submillimeter galaxies are already included in the extinction-corrected rest-frame UV star formation history, or whether their contributions need to be added on separately, as was the case for the bright submillimeter galaxies. We might expect submillimeter galaxies to become less dusty as we move to fainter submillimeter fluxes, because the spectral energy distributions become more UV dominated for lower infrared luminosities (Chary & Elbaz 2001). To test whether the faint submillimeter galaxy population follows this expectation, which would imply substantial overlap with the optically selected population, we need to determine what fraction of faint submillimeter galaxies are detected in the optical.

For this analysis, accurate positions from the SMA for the faint submillimeter galaxies are critical both for finding the correct counterparts at other wavelengths and for determining accurate amplifications and fluxes. In Chen et al. (2014), we obtained SMA detections of five faint submillimeter galaxies discovered in SCUBA images of three massive lensing cluster fields. All have de-lensed fluxes of <1 mJy with total infrared luminosities 10^10-10^11 L_Sun, comparable to LIRGs and normal star-forming galaxies. However, most of these are faint in the optical and near-infrared. This preliminary work suggests that there is a population of high-redshift, ultra-dusty galaxies with far-infrared luminosities in the LIRG range that are not being accounted for in current measurements of the star formation history.

REFERENCES

- Barger, A. J., Cowie, L. L., Chen, C.-C., Owen, F. N., Wang, W.-H., Casey, C. M., Lee, N., Sanders, D. B., & Williams, J. P. 2014, ApJ, 784, 9
- Barger, A. J., Wang, W.-H., Cowie, L. L., et al. 2012, ApJ, 761, 89
- Bouwens, R. J., Illingworth, G. D., Franx, M., et al. 2009, ApJ, 705, 936
- Chapman, S. C., Scott, D., Steidel, C. C., et al. 2000, MNRAS, 319, 318
- Chary, R., & Elbaz, D. 2001, ApJ, 556, 562
- Chen, C.-C., Cowie, L. L., Barger, A. J., Wang, W.-H., & Williams, J. P. 2014, ApJ, 789, 12
- Chen, C.-C., Cowie, L. L., Barger, A. J., et al. 2013, ApJ, 776, 131
- Holland, W. S., Bintley, D., Chapin, E. L., et al. 2013, MNRAS, 430, 2513
- Hopkins, A. M., & Beacom, J. F. 2006, ApJ, 651, 142
- Kennicutt, R. C. 1998, ApJ, 498, 541
- Peacock, J. A., Rowan-Robinson, M., Blain, A. W., et al. 2000, MNRAS,318, 535
- Reddy, N. A., Dickinson, M., Elbaz, D., et al. 2012, ApJ, 744, 154
- Reddy, N. A., & Steidel, C. C. 2009, ApJ, 692, 778
- van der Burg, R. F. J., Hildebrandt, H., & Erben, T. 2010, A&A, 523, A74
- Webb, T. M., Eales, S., Foucaud, S., et al. 2003, ApJ, 582, 6

DYNAMICAL STRUCTURE OF THE INNER 100 AU OF THE DEEPLY EMBEDDED PROTOSTAR IRAS 16293-2422

C. Favre, J. K. Jørgensen, D. Field, C. Brinch, S. Bisschop, T. L. Bourke, M. R. Hogerheijde, and W. W. Frieswijk

One of the most important questions in the study of low-mass star and planet formation is how and when circumstellar disk formation occurs, since planets form in these disks. More specifically, the collapse of a dense rotating prestellar core gives rise to a centrifugal disk. However, the presence of a magnetic field can lead to the formation of a magnetically supported pseudo-disk around a young stellar object. Contrary to a usual disk a magnetic pseudo-disk is not governed by a centrifugal balance but rather by magnetic compression. Typically, a magnetic pseudo-disk grows continually as material is accreted, and thus is generally much more massive and larger (e.g. Terebey et al. 1984, Basu 1998) than a rotation disk. The understanding of early disk formation requires, among other aspects, access to the relative

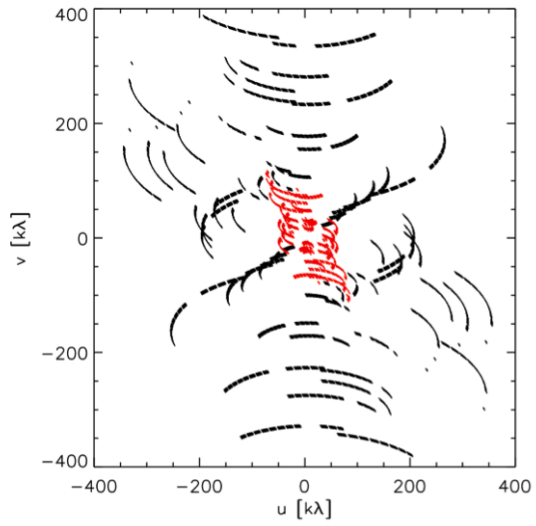

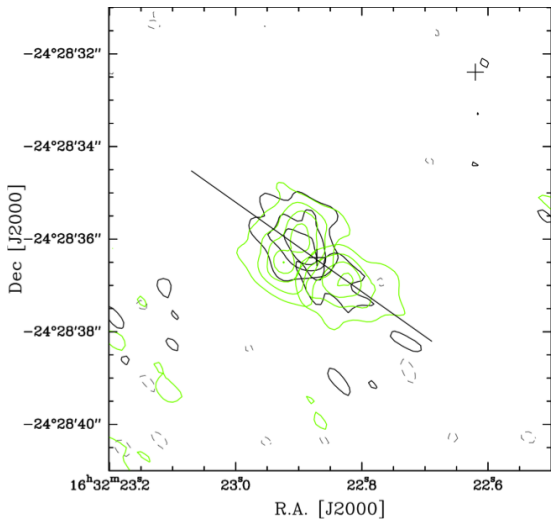

Figure 1 (left): (u,v) coverage at 337 GHz of the combined data set from the observed eSMA tracks (black lines) with the observed SMA tracks (red lines). **Figure 2 (right):** Integrated $C^{17}O$ (black) and $C^{34}S$ (green) emission map. The blueshifted emission is integrated over the velocity channels from v_{LSR} = –2.6 to 0.7 km/s and the redshifted emission between 6.6 and 9.0 km/s. The first contour and the level step are at 2σ. The full black line indicates the orientation of the northeast–southwest gradient (P.A. ~ 54°). Crosses indicate the positions of the sources IRAS 16293A and IRAS 16293B associated with Class 0 protostar IRAS 16293-2422.

importance of rotation and magnetically modified infall in protostellar objects.

Investigation of the kinematics of the gas around low-mass protostars is possible through high (sub)millimeter angular molecular resolution observations. We have performed a subarcsecond (0.59"x 0.38", i.e. ~71 x 46 AU) interferometric study of the velocity structure of the deeply low-mass Class 0 protostar IRAS 16293-2422 (located at 120 pc) using combined SMA and eSMA observations of $C^{17}O$ (3-2) and $C^{34}S$ (7-6) transitions at 337 GHz to recover both compact and extended emission (see the resulting (u,v) coverage on **Figure 1**).

Our observations show that the bulk of the $C^{17}O$ (3-2) and $C^{34}S$ (7-6) emission is associated with a velocity gradient oriented along a northeast-southwest (NE-SW) direction with P.A. of about 54º, as illustrated in **Figure 2**. A position-velocity diagram analysis shows that the velocity field on the 50-400 AU scale is *i)* consistent with a rotating structure but *ii)* inconsistent with pure Keplerian rotation. Our analysis strongly suggests that to explain the observed velocity field it is necessary to take into account the enclosed envelope mass, at the radii where the observed $C^{17}O$ and $C^{34}S$ lines are excited. We infer that this finding might result from the presence of a magnetic field and that IRAS 16293-2422 might potentially hold a pseudo-disk in formation.

REFERENCES

- Basu, S. 1998, ApJ, 509, 229
- Favre et al. 2014, ApJ, 790, 55
- Terebey et al. 1984, ApJ, 286, 529

TRANSITION FROM THE INFALLING ENVELOPE TO THE KEPLERIAN DISK AROUND L1551 IRS 5

Ti-Lin Chou & Shigehisa Takakuwa (ASIAA)

Keplerian-rotating circumstellar disks are considered to be the nurseries of planetary systems. Recent high-resolution interferometric observations have found Keplerian disks around young protostars (Jørgensen et al. 2009; Takakuwa et al. 2012; Tobin et al. 2012; Takakuwa et al. 2013; Yen et al. 2013; Ohashi et al. 2014; Takakuwa et al. 2014; Yen et al. 2014); however, it remains controversial as to how these disks are formed out of the surrounding protostellar envelopes, which often show infalling and rotating gas motions (Ohashi et al. 1997; Momose et al. 1998; Takakuwa et al. 2013; Ohashi et al. 2014; Yen et al. 2014). Direct imaging of the transition from infalling envelopes to Keplerian disks is crucial to clarify the mechanism of formation and growth of Keplerian circumstellar disks.

We have performed SMA observations of L1551 IRS 5, a Class I protobinary system with the projected separation of ~40 AU (e.g., Lim & Takakuwa 2006), in the 343 GHz continuum and CS (J =7–6) emission (Chou et al. 2014). The CS (7–6) data were taken in both the SMA subcompact and extended configurations, and furthermore combined with the single-dish mapping data taken with the Atacama Submillimeter Telescope Experiment (ASTE) (Takakuwa & Kamazaki 2011). Previous studies of L1551 IRS 5 have found active radio jets along the northeast to southwest direction (Rodríguez et al. 2003), and a ~2500-AU scale protostellar envelope in the $C^{18}O$ (1–0) emission, which exhibits infall with a conserved rotational angular momentum (Momose et al. 1998). Our SMA early science study of L1551 IRS 5 (Takakuwa et al. 2004) found rotation-dominant gas motion in the inner ~400 AU scale of the protostellar envelope, suggesting the presence of a Keplerian disk, however, the lower angular resolution in the SMA early science study prevented us from unambiguously identifying the disk. With our new SMA observations at a subarcsecond (0″.90 × 0″.65; P.A. = 82°) resolution, we have successfully identified the inner Keplerian disk and the transition from the outer infalling envelope.

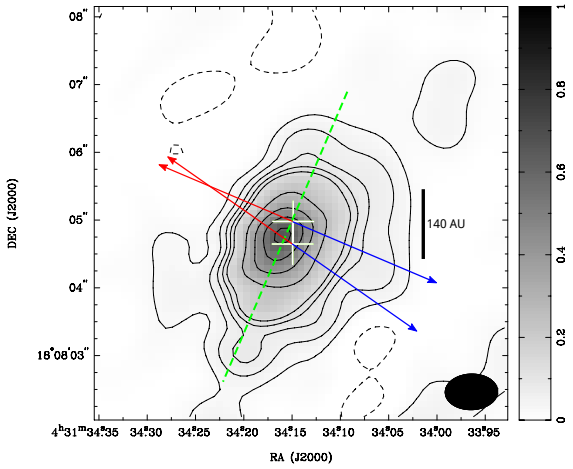

Figure 1: 343 GHz continuum image of L1551 IRS 5 observed with the SMA (contours and gray scale). Crosses denote the positions of the protobinary. A green dashed line shows the major axis, and blue and red arrows the direction of the blueshifted and redshifted jets driven by the protobinary.

Figure 1 shows the observed 343 GHz continuum image of L1551 IRS 5, which exhibits an elliptical shape elongated along the northwest-southeast direction. From the 2-dimensional Gaussian fitting to the continuum image, the size and position angle of the continuum emission are measured to be ~160 × 80 AU and P.A. = –23°, respectively. The direction of the major axis (green dashed line in Figure 1) is almost perpendicular to the associated radio jets. The continuum emission most likely traces the circumbinary disk around L1551 IRS 5, as will be proven below by the analysis of the gas motion associated with the continuum emission. From the ratio of the minor axis to the major axis,

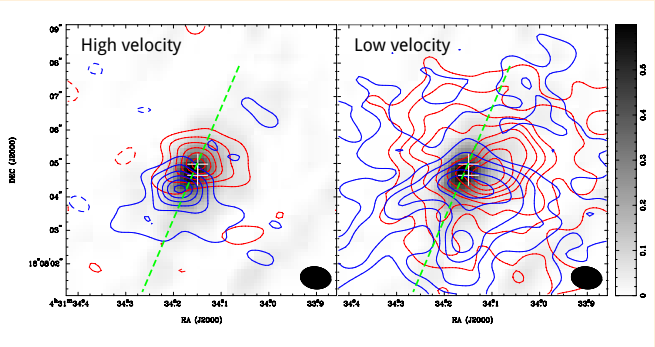

Figure 2: Distributions of the high-velocity (≳ 1.5 km s^{-1}) and low-velocity blueshifted (blue contours) and redshifted (red contours) CS (7–6) emission superposed on the 343 GHz continuum image (grey scale) in L1551 IRS 5.

the inclination angle from the plane of the sky is derived to be $i \sim \cos^{-1}(\frac{80\ \mathrm{AU}}{100\ \mathrm{AU}}) \sim 60^{\circ}$. The mass of the disk is estimated from the total continuum flux as ~0.07 $M_{\odot}$.

Figure 2 shows the integrated-intensity maps of the CS emission (blue and red contours) in the high-velocity (≳ 1.5 km s^{-1}; left) and low-velocity ranges (right) separately, superposed on the 343 GHz dust continuum image in gray scale. In the high-velocity range, the CS emission exhibits a southeast (blue) to northwest (red) velocity gradient along the major axis of the circumbinary material as seen in the 343 GHz dust continuum emission. Furthermore, the extent of the high-velocity CS emission is consistent with that of the continuum emission, suggesting that the high-velocity CS emission traces gas motion in the continuum emission. In the low-velocity range, on the other hand, the blueshifted and redshifted CS emission are extended and overlap with each other, but the centroid position of the blueshifted emission appears to be located slightly to the south of the protobinary, and that of the redshifted emission to the north.

To understand the velocity structure of the high-velocity CS emission, we performed model fittings of a geometrically-thin Keplerian disk to the observed velocity channel maps (**Figure 3** top), adopting the disk inclination angle $i = -60^{\circ}$ as measured above and the systemic velocity $v_{sys} = 6.6$ km s^{-1}. After running ~200 sets of different parameters, the best-fit Keplerian-disk model yields the central stellar mass $M_{*} = 0.5^{+0.6}_{-0.2} M_{\odot}$ and position angle of the disk $\theta = -33^{\circ}$. Middle and bottom panels of Figure 3 show the velocity channel maps of the best-fit Keplerian disk model and the residuals, respectively. The residual velocity channel maps do not show any systematic features, and the rms of the residual maps is close to the noise level of the observed velocity channel maps. The derived position angle of the Keplerian disk ($\theta = -33^{\circ}$) is consistent with the major axis of the 343 GHz continuum emission ($\theta = -23^{\circ}$), and approximately perpendicular to the axes of the jets driven by the protobinary. These results show that the observed 343 GHz continuum emission and high-velocity CS emission trace a Keplerian disk surrounding the L1551 IRS 5 binary system.

We then discuss the nature of the low-velocity CS emission in L1551 IRS 5. **Figure 4** (top) shows the observed Position-Veloci-

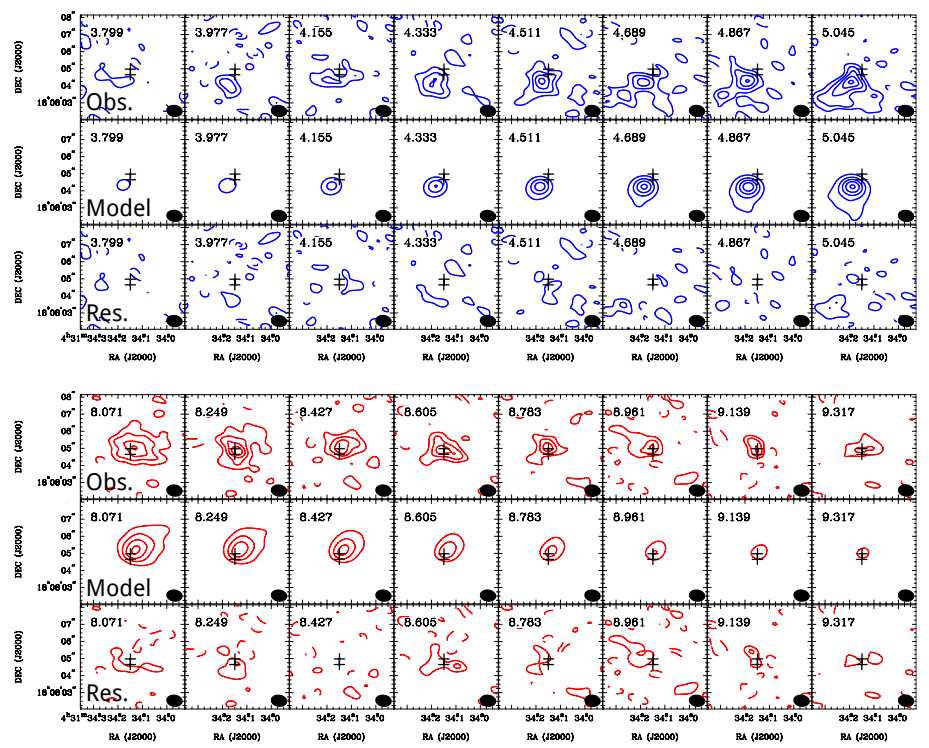

Figure 3: Best-fit results of the geometrically-thin Keplerian disk model to the observed CS (7–6) velocity channel maps at the highly blueshifted (blue contours) and redshifted (red contours) velocities in L1551 IRS 5.

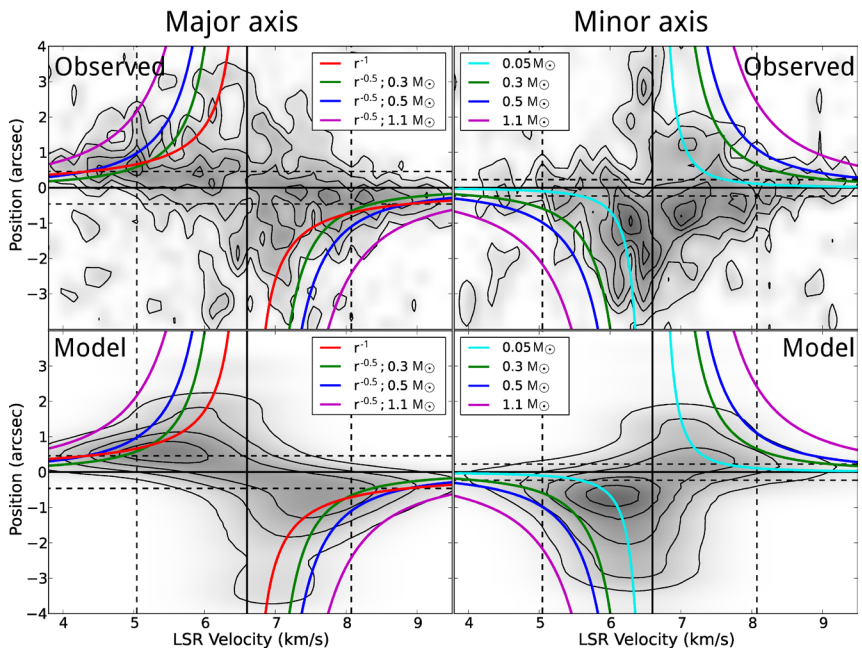

Figure 4: Observed (top) and model (bottom) P-V diagrams of the CS (7–6) emission along the major (left) and minor axes (right) of the Keplerian circumbinary disk in L1551 IRS 5. Horizontal thick and dashed lines denote the centroid position of the continuum emission and the radius of the Keplerian disk (= 64 AU). Vertical thick and dashed lines denote the systemic velocity (= 6.6 km s^{-1}) and the velocity borderline used to separate the high-velocity and low-velocity components. In the left panels, the red curves show the rotation curve with a conserved angular momentum (j= 168 AU km s^{-1}), and the green, blue, and purple curves show the Keplerian rotation curves with the central stellar masses of 0.3, 0.5, and 1.1 $M_\odot$, respectively. In the right panels, cyan, green, blue, and purple curves show free-fall gas motions with the central stellar masses of 0.05, 0.3, 0.5, and 1.1 $M_\odot$, respectively.

ty (P-V) diagrams of the CS (7–6) emission along the major (top left) and minor axes (top right). In the P-V diagram along the major axis, the velocity gradient along the southeast (blueshifted) to the northwest (redshifted) direction is evident both within and outside of the Keplerian-disk region (horizontal dashed lines). To contrast the velocity feature of the outer lower-velocity emission from that of the inner Keplerian disk, curves of two kinds of rotations are drawn in the P-V diagram along the major axis. One is the rotation with the conserved angular momentum (i.e., $v_{rot} \sim r^{-1}$), found in the ~2500 AU scale $C^{18}O$ infalling envelope by Momose et al. (1998) (red curves in Figure 4), and the other the Keplerian rotation derived above with the central stellar masses of $M_* = 0.5^{+0.6}_{-0.2} M_\odot$ (green, blue, and purple curves in Figure 4). While the Keplerian rotation curves trace the high-velocity CS emission as expected, the Keplerian rotation curves are inconsistent with the outer low-velocity emission, and the rotation with the conserved angular momentum derived from the outer ~2500 AU scale envelope appears to better trace the velocity feature of the lower-velocity CS emission. On the other hand, in the P-V diagram along the minor axis there appears a northeast (red) to southwest (blue) velocity gradient in the lower-velocity CS emission. Since the associated bipolar outflows are blueshifted to the southwest and redshifted to the northeast (Moriarty-Schieven et al. 2006; Wu et al. 2009), the near-side of the flattened envelope is northeast and the far-side southwest, and the redshifted emission on the near-side and the blueshifted emission on the far-side imply infalling motion in this envelope. The blue, purple, and green curves in Figure 4 show free-fall curves with the central stellar mass and the error bars derived from the Keplerian fitting to the high-velocity CS emission (i.e., $0.5^{+0.6}_{-0.2} M_\odot$). It is evident that the free-fall curves with the best-fit value M_*= 0.5 $M_\odot$, and even with the lower end (M_*= 0.3 $M_\odot$), do not trace the emission ridge in the P-V diagram along the minor axis. If, for example, the central stellar mass is reduced by one order of magnitude (i.e., 0.05 $M_\odot$), the free-fall curves (cyan curves in Figure 4) trace the bulk of the CS emission ridge much better. These results show that the observed infalling motion is much slower than the free-fall motion onto the central stellar mass derived from the Keplerian rotation.

In summary, the submillimeter CS emission in L1551 IRS 5 traces primarily two distinct components. One is a compact Keplerian circumbinary disk, and the other an extended envelope with the reduced infalling velocity and rotational motion of the conserved angular momentum. The lower panels of Figure 4 show P-Vs of our toy model that incorporates these components and well reproduces the main features of the observed P-Vs. The rotational motion of the infalling envelope connects smoothly to the inner Keplerian disk at ~64 AU, and the infalling motion of the envelope is reduced as the matter approaches close to the centrifugal radius. Our observations have shown direct evidence for ongoing process of disk formation and growth, which is considered to be the initial stage of planet formation. As the latest ALMA image of a Class I-II star HL Tau shows, planet formation may proceed at as early as protostellar stages. Our next aim is to search for signs of planet formation in the Keplerian disks around protostellar sources.

REFERENCES

- Chou, T.-L., Takakuwa, S., Yen, H.-W., Ohashi, N., & Ho, P. T. P. 2014, ApJ, 796, 70
- Jørgensen, J. K., van Dishoeck, E. F., Visser, R., et al. 2009, A&A, 507, 861
- Lim, J., & Takakuwa, S. 2006, ApJ, 653, 425
- Momose, M., Ohashi, N., Kawabe, R., Nakano, T., & Hayashi, M. 1998, ApJ, 504, 314
- Moriarty-Schieven, G. H., Johnstone, D., Bally, J., & Jenness, T. 2006, ApJ, 645, 357
- Ohashi, N., Hayashi, M., Ho, P. T. P., et al. 1997, ApJ, 488, 317
- Ohashi, N., Saigo, K., Aso, Y., et al. 2014, ApJ 2014, ApJ, 796, 131
- Rodríguez, L. F., Porras, A., Claussen, M. J., et al. 2003, ApJ, 586, L137
- Takakuwa, S., Ohashi, N., Ho, P. T. P., et al. 2004, ApJ, 616, L15
- Takakuwa, S., & Kamazaki, T. 2011, PASJ, 63, 921
- Takakuwa, S., Saito, M., Lim, J., et al. 2012, ApJ, 754, 52
- Takakuwa, S., Saito, M., Lim, J., & Saigo, K. 2013, ApJ, 776, 51
- Takakuwa, S., Saito, M., Saigo, K., et al. 2014, ApJ, 796, 1
- Tobin, J. J., Hartmann, L., Chiang, H.-F., et al. 2012, Nature, 492, 83
- Wu, P.-F., Takakuwa, S., & Lim, J. 2009, ApJ, 698, 184
- Yen, H.-W., Takakuwa, S., Ohashi, N., & Ho, P. T. P. 2013, ApJ, 772, 22
- Yen, H.-W., Takakuwa, S., & Ohashi, N., et al. 2014, ApJ, 793, 1

DEVELOPMENT OF YIG-BASED LOCAL OSCILLATOR MODULE FOR THE SMA

Edward Tong, Steve Leiker, Todd Hunter and Robert Kimberk

The current Local Oscillator (LO) modules in use at the SMA are based on a Gunn oscillator followed by a submillimeter frequency multiplier. There are a number of advantages of such a system, including high frequency purity, low spurious interference, robustness and simplicity. Such Gunn-based LOs have served the SMA well over the past 10+ years of operation. However, these Gunn oscillators use two mechanical tuners for their operation, and proper phase locking requires setting the tuners at the right positions. Sometimes, false locks can result, and at times, phase-locking is not even possible if one or both of the tuners lose their reference positions.

In anticipation of the upcoming 210-270 GHz receivers for the SMA, the Submillimeter Receiver Lab has begun an effort to develop a YIG-based Local Oscillator module. The goal is to produce a module that is compatible with the existing Gunn-based modules, and yet offers the same robustness, simple construction and spurious-free operation.

A photo of the experimental module is shown in **Fig. 1**. The primary source of the unit is an 8-18 GHz extremely low phase noise YIG oscillator. A YIG-control box controls the coarse tune coil of the oscillator. The output of this oscillator drives a frequency doubler, which in turn is amplified by a 22 – 30 GHz power amplifier, delivering an output power of about +24 dBm. This is the only power amplifier in the module and it is set to run very close to saturation to reduce thermal noise. Careful filtering is introduced before and after the power amplifier to reduce any harmonic interference.

The power amplifier drives a WR-12 frequency tripler, which generates 7-10 mW between 66 and 90 GHz. A coupler and harmonic mixer are inserted at the output of the tripler for phase locking purposes. The set up here is similar to the Gunn-based units, except that the Phase-Lock-Loop (PLL) acts on the FM coil of the YIG oscillator rather than the Gunn oscillator bias voltage. Finally a WR-3.4 frequency tripler takes the 66-90 GHz pumping power to produce > 0.3 mW of output power over the frequency range of 198-270 GHz. A WR-3 mechanical attenuator sets the optimal LO drive level to the SIS mixers. Laboratory tests demonstrate that there was virtually no change of receiver noise temperature at high IF. At IF below 6 GHz, there is a small increase of receiver noise by a few K due to thermal noise generated by the LO unit.

A prototype LO module was tested at the SMA in the fall. The unit was installed in the 300 GHz LO bay of antenna 1. The array was operated at an LO frequency of 267 GHz. Except for antenna 1, the regular SMA Gunn-based LO was set to operate with a Gunn frequency of 89 GHz while the YIG-based module in antenna 1 operated with a YIG frequency of 14.833 GHz. The 300 GHz receivers were used to

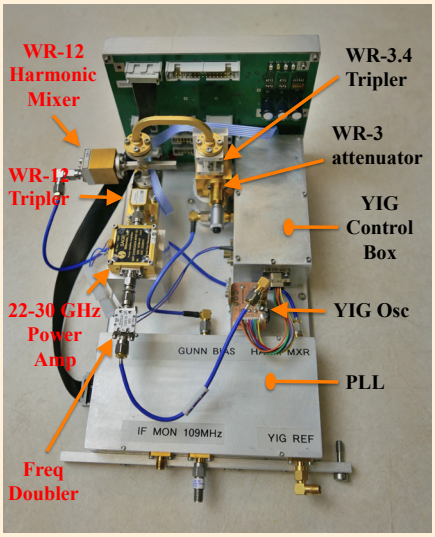

Figure 1: Photo of the YIG-based LO module. The total frequency multiplication in the module is 18, from the YIG oscillator to the final output from the WR-3.4 frequency tripler.

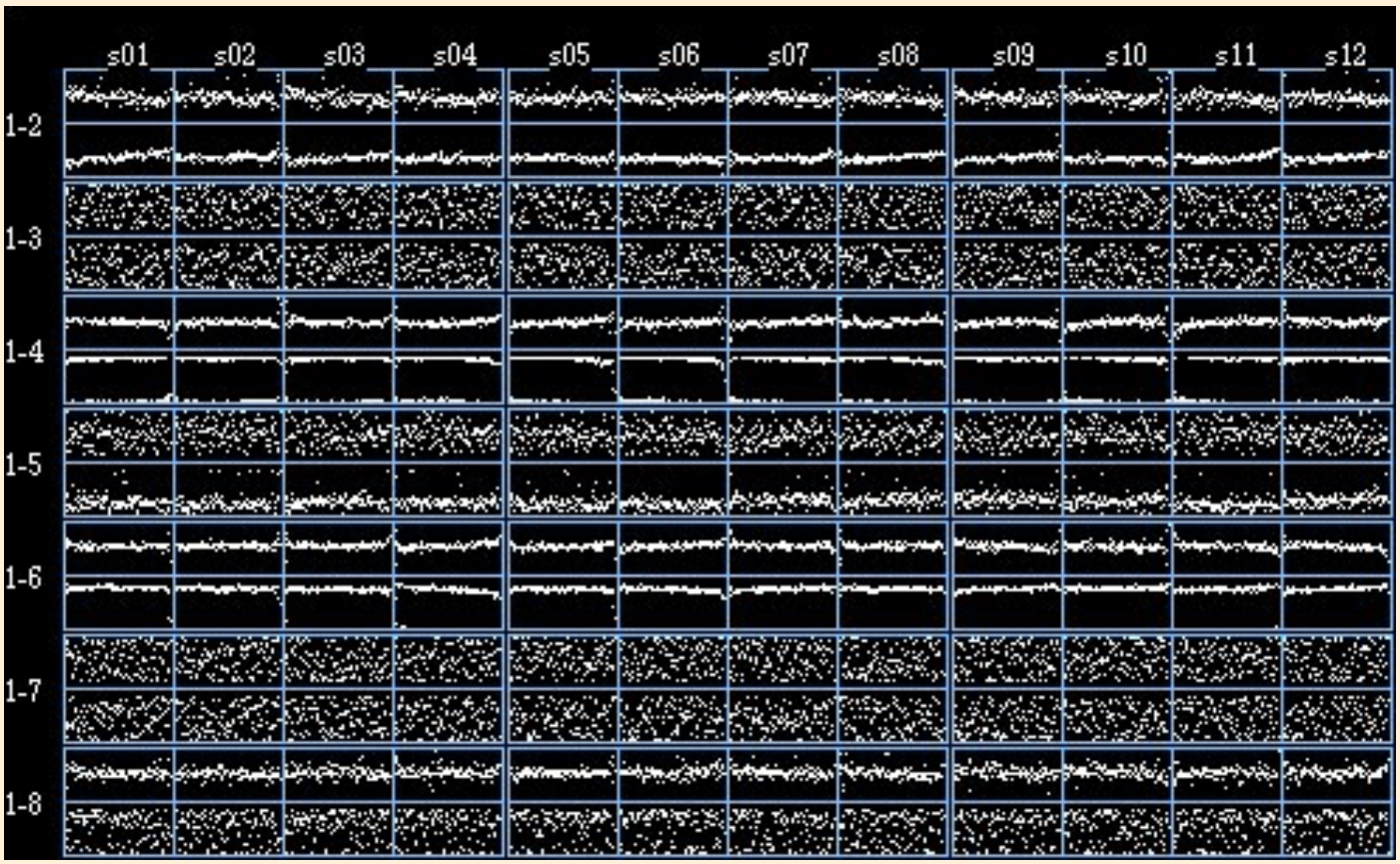

Figure 2: Correlator output showing visibility phase a function of frequency in the first 12 spectral chunks, for baselines to antenna 1. Strong fringes were observed for baselines 1-2, 1-4, and 1-6, with somewhat weaker fringes for 1-5 and 1-8 baselines. Antennas 3 and 7 were not in operation at the time of the test observation which took place on September 24, 2014. The source was Jupiter and the LO frequency was 267 GHz.

observe Jupiter. As can be seen from **Fig. 2**, stable fringes were observed on baselines involving antenna 1 in which the YIG-based LO was installed. This exercise confirms that the YIG-based LO is a viable candidate for the upcoming 210-270 GHz receiver. Further engineering effort is under way to make this module more robust for continuous operation at the SMA.

A SPECTROMETER TO MEASURE THE SPECTRAL DENSITY OF SYSTEM TEMPERATURE

Robert Kimberk, John Test, Steve Leiker, Alexander Kailash Faris

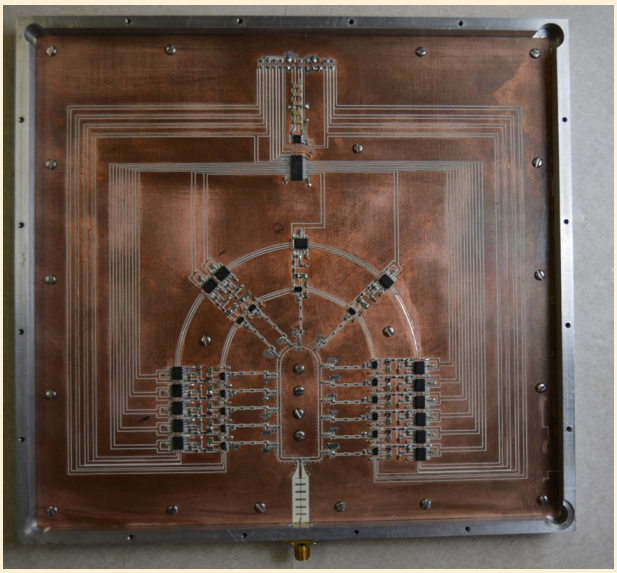

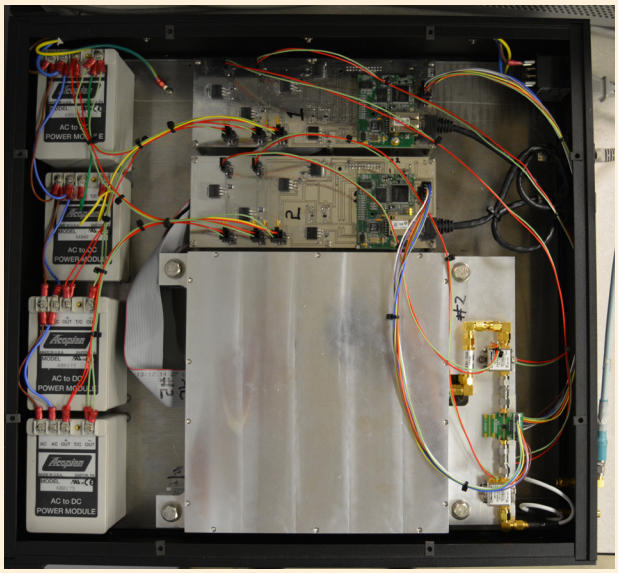

Figure 1 (left): Picture of analog autocorrelator with cover removed. Signal from SMA receiver enters the bottom and passes through a twelve GHz low pass filter. Fifteen lag power detectors surround the central delay line. At the top a signal multiplexer and amplifier send selected lag signal to Rabbit microcontroller to be digitized and averaged.

Figure 2 (right): Picture of dual channel autocorrelator rack enclosure with top removed. Two analog autocorrelators stacked at bottom of image. Two Rabbit microcontrollers at top and power supplies at left side of image. Signals from SMA receiver and Ethernet communications enters from right.

A spectrometer has been developed to measure the system temperature for each receiver of the Submillimeter Array. The spectrometer covers the new four to twelve GHz IF bandwidth. It is designed to measure the power in ten spectral bands in one second and determine a Y factor to 2% rms. The system temperature estimates will be used to generate multiplicative weights of the receiver output for the new SWARM correlator. The power data returned from the continuum detector will provide information that can be used to emphasize the portions of the observed band that provide the highest signal to noise ratios.

The Y factor is the ratio of the measured spectral power of an observed 300 K load and the observed spectral power of the sky. The system temperature is a measure of both the receiver temperature and the atmospheric noise temperature.

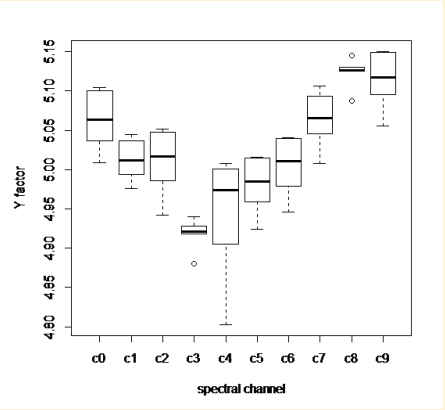

Figure 3: The results of six measurements of Y factor using a calibrated white noise source, taken over two days. The theoretical Y factor should be 5.012.

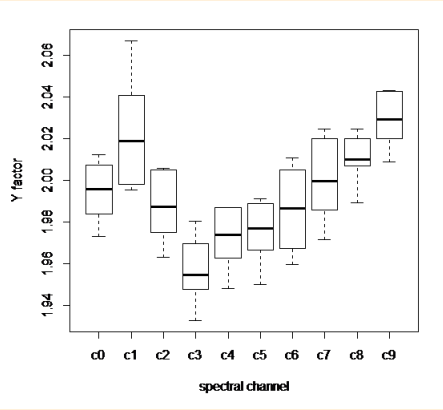

Figure 4: Represents the residual bias and variation of the six observations in each of the ten spectral channels. The theoretical Y factor should be 1.995.

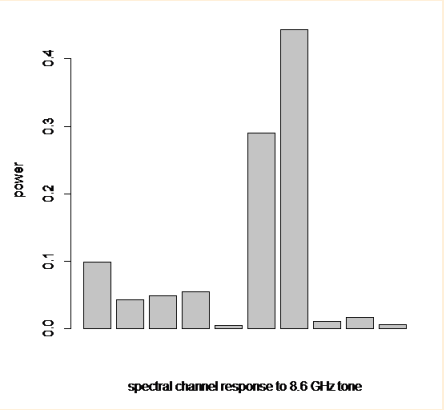

Figure 5: Bar chart of the response of the spectrometer to a 8.7 GHz tone.

The receiver temperature is a function of a number of tuning and operation variables and the atmospheric noise temperature is an uncontrolled random variable.

The new SMA spectrometer is an analog autocorrelator with fifteen lags. It splits the input signal into two halves, launches the two signals into both ends of a u-shaped coplanar waveguide and forms a standing wave. The power along the standing wave is sampled at fifteen locations [along the coplanar waveguide]. The power spectral density is computed by taking the Fourier transform of the measured lag powers. This is an application of Norbert Wiener and Aleksandr Khinchin's theorem that states that the power spectral density is the Fourier transform of the autocorrelation function. This autocorrelator is an adding interferometer which, by design, has a large DC term in the Fourier transform. This term lies outside the spectral band of interest for the SMA.

Each antenna cabin will have two spectrometers one for each of the high and low frequency receivers. The software designed to operate the spectrometer resides in the antenna PowerPC computer to allow updates to the code from remote sites. Within each spectrometer a Rabbit microcontroller digitizes and averages the lag voltages, and communicates to the antenna computer through an Ethernet link. The Rabbit also controls a digital step attenuator that is used to optimize the RF power level into the autocorrelator during observations and control the power when collecting data during the calibration sequence.

The instance directories of the PowerPCs will store configuration and calibration data for each of autocorrelators. Power data collected from the autocorrelator will be written to reflective memory in two second intervals. A calibration routine for each autocorrelator will be run once a day during the priming sequence.

THE 26TH INTERNATIONAL SYMPOSIUM ON SPACE TERAHERTZ TECHNOLOGY

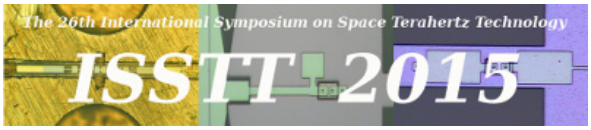

http://www.cfa.harvard.edu/ISSTT2015/

The 26th International Symposium on Space Terahertz Technology (ISSTT 2015) is jointly organized by the Smithsonian Astrophysical Observatory and the Harvard College Observatory. It will take place from March 16th through March 18th 2015 at the Knafel Center in the Radcliffe Yard on the Harvard University campus in Cambridge Massachusetts. The meeting will focus on millimeter, submillimeter, and Terahertz technology and applications, including:

- **Ultra-sensitive detectors**
- **Sources and instrumentation**
- **Optical design and measurement techniques**
- **Back end signal processors**
- **Applications of receivers and detector systems**

The Symposium has played an important role in the technological development of low noise detector/receiver systems for astrophysical applications in the millimeter and submillimeter wavelengths and all the way to the emerging Terahertz frequency band. Past proceedings of the symposium are available online (http://www.nrao.edu/meetings/isstt/).

A number of staff members of the SMA team are participating in the organization of this year's symposium. Please refer to the symposium website for more details. Registration is open. We look forward to your participation.

LOCAL ORGANIZING COMMITTEE MEMBERS

- Raymond Blundell, Chair (SAO, Harvard University)
- Colin Bischoff (Harvard University)
- Irene Coyle (Harvard University)
- Paul Grimes (SAO)
- John Kovac (Harvard University)
- Patricia Mailhot (SAO)
- Scott Paine (SAO)
- Margaret Simonini (SAO)
- Edward Tong (SAO)
- Lingzehn Zeng (SAO)

SCIENTIFIC ORGANIZING COMMITTEE MEMBERS

- Andrey Baryshev (Space Research Organization of Netherlands, The Netherlands)
- Victor Belitsky (Chalmers University, Sweden)
- Raymond Blundell (Smithsonian Astrophysical Observatory, USA)
- Gregory Gol'tsman (Moscow State Pedagogical University, Russia)
- Jeffrey Hesler (Virginia Diodes Inc., USA)
- John Kovac (Harvard University, USA)
- Imran Mehdi (Jet Propulsion Lab, USA)
- Scott Paine (Smithsonian Astrophysical Observatory, USA)
- Yutaro Sekimoto (National Astronomical Observatory of Japan, Japan)
- Edward Tong (Smithsonian Astrophysical Observatory, USA)
- Ghassan Yassin (University of Oxford, UK)

CALL FOR SMA SCIENCE OBSERVING PROPOSALS

The joint CfA-ASIAA SMA Time Allocation Committee (TAC) will issue a call for proposals in January 2015 for the observing period from 2015 May 16 through 2015 Nov 15 (2015A semester). The SMA Observer Center is expected to open for proposal submission on 2015 January 20 with an anticipated deadline for submission on 2015 February 12. For more information please see link below.

http://sma1.sma.hawaii.edu/proposing.html

The deadline for the following semester (2015 Nov 16 - 2016 May 15) is expected to be on August 6, 2015.

PROPOSAL STATISTICS 2014A (16 NOV 2014 – 15 MAY 2015)

The SMA received a total of 87 proposals (SAO 83, UH: 4) requesting observing time in the 2014B semester. The proposals received by the joint SAO and ASIAA Time Allocation Committee are divided among science categories as follows:

Category	Proposals
high mass (OB) star formation, cores	25
protoplanetary, transition, debris disks	14
submm/hi-z galaxies	13
local galaxies, starbursts, AGN	12
high mass (OB) star formation, cores	10
evolved stars, AGB, PPN	5
GRB, SN, high energy	2
solar system	1
other	1
UH	4

TRACK ALLOCATIONS BY WEATHER REQUIREMENT (ALL PARTNERS):

PWV[1]	SAO+ASIAA	UH[2]
< 4.0mm	7A + 21B	2
< 2.5mm	28A + 30B	12
< 1.0mm	0A + 0B	0
Total	**35A + 51B**	**14**

(1) Precipitable water vapor required for the observations.

(2) UH does not list As and Bs.

TOP-RANKED SAO AND ASIAA PROPOSALS - 2014B SEMESTER

The following is the listing of all SAO and ASIAA proposals with at least a partial A ranking with the names and affiliations of the principal investigators.

EVOLVED STARS, AGB, PPN

Chien-De Lee, Institute of Astronomy National Central University
Dust Formation in Evolved Massive Main Sequence Stars – Resolving the Disk Structure in the Classical Be Star FS CMa

HIGH MASS (OB) STAR FORMATION, CORES

R.M. Crutcher, UIUC
CN Zeeman Mapping of Magnetic Field Strengths

Vivien Huei-Ru Chen, National Tsing Hua University
Exploring Interactions between Magnetic Fields and Massive Young Stellar Objects

LOCAL GALAXIES, STARBURSTS, AGN

Keiichi Asada, ASIAA
Mass Accretion Rate onto the SMBH of nearby Radio Galaxies with mm/submm polarimetry

Sheperd Doeleman, SAO
Polarimetric VLBI with the Event Horizon Telescope

LOW/INTERMEDIATE MASS STAR FORMATION, CORES

Naomi Hirano, ASIAA
Magnetic fields in the earliest stage of low-mass star formation

Naomi Hirano, ASIAA
Spatio-Kinematic Structure of the HH 114 MMS outflow

Shigehisa Takakuwa, ASIAA
Circumbinary Rings and Mass Accretion onto Protostellar Binary Systems

PROTOPLANETARY, TRANSITION, DEBRIS DISKS

David Wilner, CfA
Search for Cometary Molecules in the beta Pictoris Debris DIsk

Jun Hashimoto, The University of Oklahoma
Potential Dust Trap in Asymmetric Transitional disks

Luca Ricci, Caltech (CfA beginning November 2014)
A Census of Circumstellar Disks in Ophiuchus

Meredith MacGregor, Harvard University
Structure of the HD 32297 Debris Disk

Sean Andrews, CfA
A Size--Luminosity Scaling for Protoplanetary Dust Disks

SUBMM/HI-Z GALAXIES

Scott Chapman, Dalhousie University
Locating the bright submillimeter galaxy population with SMA in northern SCUBA-2 CLS fields

ALL SAO PROPOSALS - 2014A SEMESTER

The following is the listing of all SAO proposals observed in the 2014A semester (16 May 2014 - 15 Nov 2014)

Sean Andrews, CfA
A Size--Luminosity Scaling for Protoplanetary Dust Disks

Alejandro Baez-Rubio , Centro de Astrobiología (CSIC-INTA)
Unveiling the nature of Orion Source I

Cara Battersby , CfA
Hidden Gems: Uncovering the Nature of Massive Starless Clumps

Scott Chapman , Dalhousie University
Locating the bright submillimeter galaxy population with SMA in northern SCUBA-2 CLS fields

Vivien Huei-Ru Chen , National Tsing Hua University
Are Dense Clumps in M17 SWex Nurturing O Stars?

Michael Dunham , CfA
Disks Around Variably Accreting Young Stars: Confirming FUor Disk Detections

Michael Dunham , CfA
The Molecular Outflow Driven by the Candidate First Hydrostatic Core Per-Bolo 45

Christopher Faesi , Harvard University
The Molecular Cloud Populations in Nearby Galaxies: NGC 300

Pau Frau , Observatorio Astronomico Nacional (OAN) - Centro de Astrobiologia (CSIC-INTA)
Assessing the role of magnetic fields in a filament with super-Jeans fragmention

Josep Miquel Girart , Institut de Ciències de l'Espai (CSIC-IEEC)
Characterizing the powering source of the short-lived, compact bipolar water maser outflow in LkHa 234

Shan Huang , ASIAA
CO and Star Formation in a HIghMass Galaxy

Meredith Hughes , Wesleyan University
HD 166191: Giant Debris Impact or Late-Stage Transition Disk?

Jes Jørgensen , Niels Bohr Institute and Centre for Star and Planet Formation
Episodic accretion and complex organics in the inner regions of protostars

Jun Yi Koay , University of Copenhagen
Has the central black hole in Mrk 590 run out of gas?

Lars Kristensen , CfA
HCN as a probe of physical conditions: constraining the chemistry in low-mass protostars

Meredith MacGregor , Harvard University
Deciphering Debris Disk Structure and Eccentricity

Dan Marrone , University of Arizona
Probing the G2 Gas Cloud Disruption by Sagittarius A with SMA and CARMA Polarimetry*

Nicole Nesvadba , Institut d'Astrophysique Spatiale Orsay
Probing intense star-formation in the brightest gravitationally lensed high-z galaxies discovered with Planck

Karin Öberg , Harvard University
A complete, spatially resolved survey of complex molecules in MYSO ice sources

Keping Qiu , Nanjing University
A twin jet powered by a massive protobinary in IRAS 16547-4247?

Keping Qiu , Nanjing University
A Toroidal Magnetic Field in the Brightest YSO Radio Jet in our Galaxy?

Vlas Sokolov , National Tsing Hua University
IRDC structure driven by cloud-cloud collision

Ren-Shiang Sung , National Tsing Hua University
CO Outflows of Very Low Luminosity Objects in Taurus

Alex Tetarenko , University of Alberta
Constraining the Jet Properties of Transient X-ray Binaries

Arthur Cheng-Hung Tsai , National Tsing Hua University
Imaging Compact Knots in Extreme High Velocity Outflows Driven by Intermediate-Mass Protostars

Wouter Vlemmings , Chalmers University of Technology
The magnetic field of binary evolved stars

Wei-Hao Wang , ASIAA
SMA Identification of Strongly Amplified SCUBA-2 Sources

David Wilner , CfA
Large Grains in the epsilon Eri Debris Disk

Hsi-Wei Yen , ASIAA
Linking velocity and magnetic-B field analyses from disks to associated clouds

Qizhou Zhang , CfA
H30 alpha & H26 alpha recombination masers in MWC349A

RECENT PUBLICATIONS

Title: Peculiar Near-Nucleus Outgassing of Comet 17P/Holmes During Its 2007 Outburst
Authors: Qi, Chunhua; Hogerheijde, Michiel R.; Jewitt, David; Gurwell, Mark A.; Wilner, David J.
Publication: *eprint arXiv:1411.4632*
Publication Date: *11/2014*
Abstract: http://adsabs.harvard.edu/abs/2014arXiv1411.4632Q

Title: The Importance of the Magnetic Field from an SMA-CSO-combined Sample of Star-forming Regions
Authors: Koch, Patrick M.; Tang, Ya-Wen; Ho, Paul T. P.; Zhang, Qizhou; Girart, Josep M.; Chen, Huei-Ru Vivien; Frau, Pau; Li, Hua-Bai; Li, Zhi-Yun; Liu, Hau-Yu Baobab; Padovani, Marco; Qiu, Keping; Yen, Hsi-Wei; Chen, How-Huan; Ching, Tao-Chung; Lai, Shih-Ping; Rao, Ramprasad
Publication: *The Astrophysical Journal, Volume 797, Issue 2, article id. 99, 17 pp. (2014). (ApJ Homepage)*
Publication Date: 12/2014
Abstract: http://adsabs.harvard.edu/abs/2014arXiv1411.3830K

Title: The Structure of Pre-transitional Protoplanetary Disks. II. Azimuthal Asymmetries, Different Radial Distributions of Large and Small Dust Grains in PDS~70
Authors: Hashimoto, J.; Tsukagoshi, T.; Brown, J. M.; Dong, R.; Takayuki Muto, Mr.; Zhu, Zhaohuan, Dr.; Wisniewski, John P., Dr.; Ohashi, N.; kudo, T.; Kusakabe, N.; Abe, L.; Akiyama, E.; Brandner, Wolfgang; Brandt, T.; Carson, J.; Currie, Thayne, Dr.; Egner, S.; Feldt, M.; Grady, C. A.; Guyon, O.; Hayano, Y.; Hayashi, M.; Hayashi, S.; Henning, Thomas; Hodapp, K.; Ishii, M.; Iye, Masanori, Dr.; Janson, M.; Kandori, R.; Knapp, G.; Kuzuhara, M.; Kwon, J.; Matsuo, T.; McElwain, M. W.; Mayama, S.; Mede, K.; Miyama, S.; Morino, J.-I.; Moro-Martin, A.; Nishimura, T.; Pyo, T.-S.; Serabyn, Gene, Dr.; Suenaga, T.; Suto, H.; Suzuki, R.; Takahashi, Y.; Takami, M.; Takato, N.; Terada, H.; Thalmann, Christian, Dr.; Tomono, D.; Turner, E. L.; Watanabe, M.; Yamada, T.; Takami, H.; Usuda, T.; Tamura, M.
Publication: *eprint arXiv:1411.2587*
Publication Date: 11/2014
Abstract: http://adsabs.harvard.edu/abs/2014arXiv1411.2587H

Title: Magnetic Field Structure in the Flattened Envelope and Jet in the Young Protostellar System HH 211
Authors: Lee, Chin-Fei; Rao, Ramprasad; Ching, Tao-Chung; Lai, Shih-Ping; Hirano, Naomi; Ho, Paul T. P.; Hwang, Hsiang-Chih
Publication: *The Astrophysical Journal Letters, Volume 797, Issue 1, article id. L9, 4 pp. (2014). (ApJL Homepage)*
Publication Date: 12/2014
Abstract: http://adsabs.harvard.edu/abs/2014ApJ...797L...9L

Title: Excitation Conditions in the Multi-component Submillimeter Galaxy SMM J00266+1708
Authors: Sharon, Chelsea E.; Baker, Andrew J.; Harris, Andrew I.; Tacconi, Linda J.; Lutz, Dieter; Longmore, Steven N.
Publication: *eprint arXiv:1411.0700*
Publication Date: 11/2014
Abstract: http://adsabs.harvard.edu/abs/2014arXiv1411.0700S

Title: Kinematics of the Outflow From The Young Star DG Tau B: Rotation in the vicinities of an optical jet
Authors: Zapata, Luis A.; Lizano, Susana; Rodriguez, Luis F.; Ho, Paul T. P.; Loinard, Laurent; Fernandez-Lopez, Manuel; Tafoya, Daniel
Publication: *eprint arXiv:1411.0173*
Publication Date: 11/2014
Abstract: http://adsabs.harvard.edu/abs/2014arXiv1411.0173Z

Title: The VLA Nascent Disk and Multiplicity (VANDAM) Survey of Perseus Protostars. Resolving the Sub-arcsecond Binary System in NGC 1333 IRAS2A
Authors: Tobin, John J.; Dunham, Michael M.; Looney, Leslie W.; Li, Zhi-Yun; Chandler, Claire J.; Segura-Cox, Dominique; Sadavoy, Sarah I.; Melis, Carl; Harris, Robert J.; Perez, Laura M.; Kratter, Kaitlin; Jørgensen, Jes K.; Plunkett, Adele L.; Hull, Charles L. H.
Publication: *The Astrophysical Journal, Volume 798, Issue 1, article id. 61, 13 pp. (2015). (ApJ Homepage)*
Publication Date: 01/2015
Abstract: http://adsabs.harvard.edu/abs/2014arXiv1410.8134T

Title: Resolving the Bright HCN(1-0) Emission toward the Seyfert 2 Nucleus of M51: Shock Enhancement by Radio Jets and Weak Masing by Infrared Pumping?
Authors: Matsushita, Satoki; Dinh-V-Trung; Boone, Frédéric; Krips, Melanie; Lim, Jeremy; Muller, Sebastien
Publication: *eprint arXiv:1410.7863*
Publication Date: 10/2014
Abstract: http://adsabs.harvard.edu/abs/2014arXiv1410.7863M

Title: Around the Ring We Go: The Cold, Dense Ring of Molecular Gas in NGC 1614
Authors: Sliwa, Kazimierz; Wilson, Christine D.; Iono, Daisuke; Peck, Alison; Matsushita, Satoki
Publication: *The Astrophysical Journal Letters, Volume 796, Issue 1, article id. L15, 7 pp. (2014). (ApJL Homepage)*
Publication Date: 11/2014
Abstract: http://adsabs.harvard.edu/abs/2014ApJ...796L..15S

Title: Probing the Parsec-scale Accretion Flow of 3C 84 with Millimeter Wavelength Polarimetry
Authors: Plambeck, R. L.; Bower, G. C.; Rao, Ramprasad; Marrone, D. P.; Jorstad, S. G.; Marscher, A. P.; Doeleman, S. S.; Fish, V. L.; Johnson, M. D.
Publication: *The Astrophysical Journal, Volume 797, Issue 1, article id. 66, 6 pp. (2014). (ApJ Homepage)*
Publication Date: 12/2014
Abstract: http://adsabs.harvard.edu/abs/2014ApJ...797...66P

Title: Transition from the Infalling Envelope to the Keplerian Disk around L1551 IRS 5
Authors: Chou, Ti-Lin; Takakuwa, Shigehisa; Yen, Hsi-Wei; Ohashi, Nagayoshi; Ho, Paul T. P.
Publication: *The Astrophysical Journal, Volume 796, Issue 1, article id. 70, 15 pp. (2014). (ApJ Homepage)*
Publication Date: 11/2014
Abstract: http://adsabs.harvard.edu/abs/2014ApJ...796...70C

Title: G11.92--0.61-MM2: A Bonafide Massive Prestellar Core?
Authors: Cyganowski, C. J.; Brogan, C. L.; Hunter, T. R.; Graninger, D.; Öberg, K. I.; Vasyunin, A.; Zhang, Q.; Friesen, R.; Schnee, S.
Publication: *The Astrophysical Journal Letters, Volume 796, Issue 1, article id. L2, 9 pp. (2014). (ApJL Homepage)*
Publication Date: 11/2014
Abstract: http://adsabs.harvard.edu/abs/2014ApJ...796L...2C

Title: NGC 7538 IRS. 1. Interaction of a Polarized Dust Spiral and a Molecular Outflow
Authors: Wright, M. C. H.; Hull, Charles L. H.; Pillai, Thushara; Zhao, Jun-Hui; Sandell, Göran
Publication: *The Astrophysical Journal, Volume 796, Issue 2, article id. 112, 5 pp. (2014). (ApJ Homepage)*
Publication Date: 12/2014
Abstract: http://adsabs.harvard.edu/abs/2014ApJ...796..112W

Title: Diversity of chemistry and excitation conditions in the high-mass star forming complex W33
Authors: Immer, K.; Galván-Madrid, R.; König, C.; Liu, H. B.; Menten, K. M.
Publication: *Astronomy Astrophysics, Volume 572, id.A63, 64 pp. (A A Homepage)*
Publication Date: 12/2014
Abstract: http://adsabs.harvard.edu/abs/2014A%26A...572A..63I

Title: Submillimeter Array Observations of Magnetic Fields in G240.31+0.07: An Hourglass in a Massive Cluster-forming Core
Authors: Qiu, Keping; Zhang, Qizhou; Menten, Karl M.; Liu, Hauyu B.; Tang, Ya-Wen; Girart, Josep M.
Publication: *The Astrophysical Journal Letters, Volume 794, Issue 1, article id. L18, 6 pp. (2014). (ApJL Homepage)*
Publication Date: 10/2014
Abstract: http://adsabs.harvard.edu/abs/2014ApJ...794L..18Q

Title: Characterization of Molecular Outflows in the Substellar Domain
Authors: Phan-Bao, Ngoc; Lee, Chin-Fei; Ho, Paul T. P.; Dang-Duc, Cuong; Li, Di
Publication: *The Astrophysical Journal, Volume 795, Issue 1, article id. 70, 7 pp. (2014). (ApJ Homepage)*
Publication Date: 11/2014
Abstract: http://adsabs.harvard.edu/abs/2014arXiv1408.4506P

Title: Molecular tendrils feeding star formation in the Eye of the Medusa. The Medusa merger in high resolution 12CO 2-1 maps
Authors: König, S.; Aalto, S.; Lindroos, L.; Muller, S.; Gallagher, J. S.; Beswick, R. J.; Petitpas, G.; Jütte, E.
Publication: *Astronomy Astrophysics, Volume 569, id.A6, 11 pp. (A&A Homepage)*
Publication Date: 09/2014
Abstract: http://adsabs.harvard.edu/abs/2014arXiv1407.8347K

Title: IC 348-SMM2E: a Class 0 proto-brown dwarf candidate forming as a scaled-down version of low-mass stars
Authors: Palau, Aina; Zapata, Luis A.; Rodríguez, Luis F.; Bouy, Hervé; Barrado, David; Morales-Calderón, María; Myers, Philip C.; Chapman, Nicholas; Juárez, Carmen; Li, Di
Publication: *Monthly Notices of the Royal Astronomical Society, Volume 444, Issue 1, p.833-845 (MNRAS Homepage)*
Publication Date: 10/2014
Abstract: http://adsabs.harvard.edu/abs/2014arXiv1407.7764P

Title: Cold Molecular Gas in Merger Remnants. I. Formation of Molecular Gas Disks
Authors: Ueda, Junko; Iono, Daisuke; Yun, Min S.; Crocker, Alison F.; Narayanan, Desika; Komugi, Shinya; Espada, Daniel; Hatsukade, Bunyo; Kaneko, Hiroyuki; Matsuda, Yuichi; Tamura, Yoichi; Wilner, David J.; Kawabe, Ryohei; Pan, Hsi-An
Publication: *The Astrophysical Journal Supplement, Volume 214, Issue 1, article id. 1, 29 pp. (2014). (ApJS Homepage)*
Publication Date: 09/2014
Abstract: http://adsabs.harvard.edu/abs/2014arXiv1407.6873U

Title: Circumbinary Ring, Circumstellar Disks, and Accretion in the Binary System UY Aurigae
Authors: Tang, Ya-Wen; Dutrey, Anne; Guilloteau, Stéphane; Piétu, Vincent; Di Folco, Emmanuel; Beck, Tracy; Ho, Paul T. P.; Boehler, Yann; Gueth, Fréderic; Bary, Jeff; Simon, Michal
Publication: *The Astrophysical Journal, Volume 793, Issue 1, article id. 10, 14 pp. (2014). (ApJ Homepage)*
Publication Date: 09/2014
Abstract: http://adsabs.harvard.edu/abs/2014arXiv1407.4561T

Title: Magnetic Fields and Massive Star Formation
Authors: Zhang, Qizhou; Qiu, Keping; Girart, Josep M.; (Baobab Liu, Hauyu; Tang, Ya-Wen; Koch, Patrick M.; Li, Zhi-Yun; Keto, Eric; Ho, Paul T. P.; Rao, Ramprasad; Lai, Shih-Ping; Ching, Tao-Chung; Frau, Pau; Chen, How-Huan; Li, Hua-Bai; Padovani, Marco; Bontemps, Sylvain; Csengeri, Timea; Juárez, Carmen
Publication: *The Astrophysical Journal, Volume 792, Issue 2, article id. 116, 12 pp. (2014). (ApJ Homepage)*
Publication Date: 09/2014
Abstract: http://adsabs.harvard.edu/abs/2014arXiv1407.3984Z

Title: The origin of organic emission in NGC 2071
Authors: van Kempen, T. A.; McCoey, C.; Tisi, S.; Johnstone, D.; Fich, M.
Publication: *Astronomy Astrophysics, Volume 569, id.A53, 9 pp. (A&A Homepage)*
Publication Date: 09/2014
Abstract: http://adsabs.harvard.edu/abs/2014arXiv1407.2426V

Title: Unusual flaring activity in the blazar PKS 1424-418 during 2008-2011
Authors: Buson, S.; Longo, F.; Larsson, S.; Cutini, S.; Finke, J.; Ciprini, S.; Ojha, R.; D'Ammando, F.; Donato, D.; Thompson, D. J.; Desiante, R.; Bastieri, D.; Wagner, S.; Hauser, M.; Fuhrmann, L.; Dutka, M.; Müller, C.; Kadler, M.; Angelakis, E.; Zensus, J. A.; Stevens, J.; Blanchard, J. M.; Edwards, P. G.; Lovell, J. E. J.; Gurwell, M. A.; Wehrle, A. E.; Zook, A.
Publication: *Astronomy Astrophysics, Volume 569, id.A40, 11 pp. (A&A Homepage)*
Publication Date: 09/2014
Abstract: http://adsabs.harvard.edu/abs/2014arXiv1407.0299B

Title: Dynamical Structure of the Inner 100 AU of the Deeply Embedded Protostar IRAS 16293-2422
Authors: Favre, Cécile; Jørgensen, Jes K.; Field, David; Brinch, Christian; Bisschop, Suzanne E.; Bourke, Tyler L.; Hogerheijde, Michiel R.; Frieswijk, Wilfred W. F.
Publication: *The Astrophysical Journal, Volume 790, Issue 1, article id. 55, 11 pp. (2014). (ApJ Homepage)*
Publication Date: 07/2014
Abstract: http://adsabs.harvard.edu/abs/2014ApJ...790...55F

Title: Two Extreme Young Objects in Barnard 1-b
Authors: Hirano, Naomi; Liu, Fang-chun
Publication: *The Astrophysical Journal, Volume 789, Issue 1, article id. 50, 18 pp. (2014). (ApJ Homepage)*
Publication Date: 07/2014
Abstract: http://adsabs.harvard.edu/abs/2014ApJ...789...50H

Title: Shaping a high-mass star-forming cluster through stellar feedback. The case of the NGC 7538 IRS 1-3 complex
Authors: Frau, P.; Girart, J. M.; Zhang, Q.; Rao, R.
Publication: *Astronomy Astrophysics, Volume 567, id.A116, 14 pp. (A&A Homepage)*
Publication Date: 07/2014
Abstract: http://adsabs.harvard.edu/abs/2014arXiv1405.6742F

Title: The Disappearing Envelope around the Transitional Class I Object L43
Authors: Koyamatsu, Shin; Takakuwa, Shigehisa; Hayashi, Masahiko; Mayama, Satoshi; Ohashi, Nagayoshi
Publication: *The Astrophysical Journal, Volume 789, Issue 2, article id. 95, 13 pp. (2014). (ApJ Homepage)*
Publication Date: 07/2014
Abstract: http://adsabs.harvard.edu/abs/2014ApJ...789...95K

Title: Synchrotron Self-inverse Compton Radiation from Reverse Shock on GRB 120326A
Authors: Urata, Yuji; Huang, Kuiyun; Takahashi, Satoko; Im, Myungshin; Yamaoka, Kazutaka; Tashiro, Makoto; Kim, Jae-Woo; Jang, Minsung; Pak, Soojong
Publication: *The Astrophysical Journal, Volume 789, Issue 2, article id. 146, 8 pp. (2014). (ApJ Homepage)*
Publication Date: 07/2014
Abstract: http://adsabs.harvard.edu/abs/2014ApJ...789..146U

Title: A Strong Radio Brightening at the Jet Base of M 87 during the Elevated Very High Energy Gamma-Ray State in 2012
Authors: Hada, K.; Giroletti, M.; Kino, M.; Giovannini, G.; D'Ammando, F.; Cheung, C. C.; Beilicke, M.; Nagai, H.; Doi, A.; Akiyama, K.; Honma, M.; Niinuma, K.; Casadio, C.; Orienti, M.; Krawczynski, H.; Gómez, J. L.; Sawada-Satoh, S.; Koyama, S.; Cesarini, A.; Nakahara, S.; Gurwell, M. A.
Publication: *The Astrophysical Journal, Volume 788, Issue 2, article id. 165, 13 pp. (2014). (ApJ Homepage)*
Publication Date: 06/2014
Abstract: http://adsabs.harvard.edu/abs/2014ApJ...788..165H

Title: A Parametric Modeling Approach to Measuring the Gas Masses of Circumstellar Disks
Authors: Williams, Jonathan P.; Best, William M. J.
Publication: *The Astrophysical Journal, Volume 788, Issue 1, article id. 59, 15 pp. (2014). (ApJ Homepage)*
Publication Date: 06/2014
Abstract: http://adsabs.harvard.edu/abs/2014ApJ...788...59W

The Submillimeter Array (SMA) is a pioneering radio-interferometer dedicated to a broad range of astronomical studies including finding protostellar disks and outflows; evolved stars; the Galactic Center and AGN; normal and luminous galaxies; and the solar system. Located on Mauna Kea, Hawaii, the SMA is a collaboration between the Smithsonian Astrophysical Observatory and the Academia Sinica Institute of Astronomy and Astrophysics.

SUBMILLIMETER ARRAY
Harvard-Smithsonian Center
for Astrophysics
60 Garden Street, MS 78
Cambridge, MA 02138 USA
www.cfa.harvard.edu/sma/

SMA HILO OFFICE
645 North A'ohoku Place
Hilo, Hawaii 96720
Ph. 808.961.2920
Fx. 808.961.2921
sma1.sma.hawaii.edu

ACADEMIA SINICA INSTITUTE OF
ASTRONOMY & ASTROPHYSICS
P.O. Box 23-141
Taipei 10617
Taiwan R.O.C.
www.asiaa.sinica.edu.tw/